2017

Elemental and mineralogical analysis of marine and coastal sediments from Phra Thong Island, Thailand: Insights into the provenance of coastal hazard deposits

Dat Pham
Nanyang Technological University

Chris Gouramanis
National Univeristy of Singapore

Adam D. Switzer
Nanyang Technological University, University of Wollongong, aswitzer@uow.edu.au

Charles Rubin
Nanyang Technological University

Brian G. Jones
University of Wollongong, briangj@uow.edu.au

See next page for additional authors

Publication Details

Pham, D. T., Gouramanis, C., Switzer, A. D., Rubin, C. M., Jones, B. G., Jankaew, K. & Carr, P. F. (2017). Elemental and mineralogical analysis of marine and coastal sediments from Phra Thong Island, Thailand: Insights into the provenance of coastal hazard deposits. Marine Geology, 385 274-292.

Elemental and mineralogical analysis of marine and coastal sediments from Phra Thong Island, Thailand: Insights into the provenance of coastal hazard deposits

Abstract
Sediment records left by coastal hazards (e.g. tsunami and/or storms) may shed light on the sedimentary and hydrodynamic processes happening during such events. Modern onshore and offshore sediment samples were compared with the 2004 Indian Ocean Tsunami, three palaeotsunami and a 2007 storm deposit from Phra Thong Island, Thailand, to determine provenance relationships between these coastal overwash deposits. Sedimentological and stratigraphic characteristics are generally inadequate to discriminate tsunami and storm deposits so a statistical approach (including cluster analysis, principal component analysis and discriminant function analysis) was used based on grain size, mineralogy and trace element geochemistry. The mineral content and trace element geochemistry are statistically inadequate to distinguish the provenance of the modern storm and tsunami deposits at this site, but the mean grain size can potentially discriminate these overwash deposits. The 2007 storm surge deposits were most likely sourced from the onshore sediment environment whereas all four tsunami units statistically differ from each other indicating diverse sediment sources. Our statistical analyses suggest that the 2004 tsunami deposit was mainly derived from nearshore marine sediments. The uppermost palaeotsunami deposit was possibly derived from both onshore and nearshore materials while the lower palaeotsunami deposits showed no clear evidence of their sediment sources. Such complexity raises questions about the origin of the sediments in the tsunami and storm deposits and strongly suggests that local context and palaeogeography are important aspects that cannot be ignored in tsunami provenance studies.

Disciplines
Medicine and Health Sciences | Social and Behavioral Sciences

Publication Details
Pham, D. T., Gouramanis, C., Switzer, A. D., Rubin, C. M., Jones, B. G., Jankaew, K. & Carr, P. F. (2017). Elemental and mineralogical analysis of marine and coastal sediments from Phra Thong Island, Thailand: Insights into the provenance of coastal hazard deposits. Marine Geology, 385 274-292.

Authors
Dat Pham, Chris Gouramanis, Adam D. Switzer, Charles Rubin, Brian G. Jones, Kruawun Jankaew, and Paul F. Carr

Elemental and mineralogical analysis of marine and coastal sediments from Phra Thong Island, Thailand: Insights into the provenance of coastal hazard deposits.

Dat T. Pham[1,2], Chris Gouramanis[3], Adam D. Switzer[1,2], Charles M. Rubin[1,2], Brian G. Jones[4], Kruawun Jankaew[5], Paul F. Carr[4]

[1]*Asian School of the Environment, Nanyang Technological University, Singapore 639798*

[2]*Earth Observatory of Singapore, Singapore 639798*

[3]*Department of Geography, Faculty of Arts and Social Sciences, National University of Singapore, Singapore 117570.*

[4]*School of Earth and Environmental Sciences, University of Wollongong, NSW 2522, Australia*

[5]*Department of Geology, Faculty of Science, Chulalongkorn University, Bangkok 10330, Thailand*

Corresponding author: Dr. Chris Gouramanis; email address: geogc@nus.edu.sg; postal address: Department of Geography, Faculty of Arts and Social Sciences, National University of Singapore, AS2-04-02, 1 Arts Link, Kent Ridge, Singapore 117570; Tel: (65) 6516 3855.

Highlights:

- Overwash deposits cannot be identified from geochemical proxies at this site

- Mineral and trace metal data sets show very complex relationships through time
- The 2004 tsunami deposit is primarily sourced from shallow marine sediments
- The provenance of prehistoric tsunami deposits is complex and remains unclear

Abstract:

Sediment records left by coastal hazards (e.g. tsunami and/or storms) may shed light on the sedimentary and hydrodynamic processes happening during such events. Modern onshore and offshore sediment samples were compared with the 2004 Indian Ocean Tsunami, three palaeotsunami and a 2007 storm deposit from Phra Thong Island, Thailand, to determine provenance relationships between these coastal overwash deposits. Sedimentological and stratigraphic characteristics are generally inadequate to discriminate tsunami and storm deposits so a statistical approach (including cluster analysis, principal component analysis and discriminant function analysis) was used based on grain size, mineralogy and trace element geochemistry. The mineral content and trace element geochemistry are statistically inadequate to distinguish the provenance of the modern storm and tsunami deposits at this site, but the mean grain size can potentially discriminate these overwash deposits. The 2007 storm surge deposits were most likely sourced from the onshore sediment environment whereas all four tsunami units statistically differ from each other indicating diverse sediment sources. Our statistical analyses suggest that the

2004 tsunami deposit was mainly derived from nearshore marine sediments. The uppermost palaeotsunami deposit was possibly derived from both onshore and nearshore materials while the lower palaeotsunami deposits showed no clear evidence of their sediment sources. Such complexity raises questions about the origin of the sediments in the tsunami and storm deposits and strongly suggests that local context and palaeogeography are important aspects that cannot be ignored in tsunami provenance studies.

Key words: tsunami deposit, storm deposit, provenance, trace elements, mineral compositions, grain size parameters, cluster analysis, principal component analysis, bootstrap analysis, discriminant function analysis.

1. Introduction

Coastal areas offer favourable conditions to support dense human populations and critical infrastructure (Syvitski et al., 2009). These areas, however, are also vulnerable to coastal hazards, of which tsunamis and storms are the most disastrous (e.g. Switzer et al., 2014). A series of such disasters have occurred in the last decade, including the 2004 Indian Ocean Tsunami (IOT), Hurricane Katrina (2005), Cyclone Nargis (2008), the Tohoku-oki earthquake-induced tsunami (2011), Hurricane Sandy (2012), Typhoon Haiyan (2013) and Hurricane Patricia (2015). These disasters highlight the need for accurate coastal vulnerability assessments including the examination of the recurrence interval of such events. Understanding the recurrence interval of these events is crucial for future risk assessment (e.g.,

71 Switzer et al., 2014). Due to the inadequate and short historical records (i.e.
72 frequently less than 100 years) in many affected areas, the geological record
73 preserved along coasts may capture a much longer timeframe and provide evidence
74 for historical occurrences and allow the determination of the recurrence intervals of
75 tsunamis (e.g. Minoura et al., 2001; Jankaew et al., 2008; Monecke et al., 2008) and
76 storms (e.g. Liu and Fearn, 2000; Nott, 2011).

77

78 Both tsunami and storm deposits are the result of overwash processes caused by
79 high-energy events, and in many cases they exhibit very similar sedimentary
80 signatures (e.g. Kortekaas and Dawson, 2007; Switzer and Jones, 2008). Thus, in
81 order to accurately assess how frequently catastrophic events affect coastal regions,
82 it is necessary to know whether the identified coastal washover deposit was caused
83 by a tsunami or a storm event (e.g. Switzer et al., 2014).

84

85 Tsunami and storm deposits have been compared in numerous studies with an
86 expectation of developing a suite of diagnostic criteria to distinguish deposits
87 formed by different coastal overwash processes (e.g. Nanayama et al., 2000; Goff et
88 al., 2004; Tuttle et al., 2004; Kortekaas and Dawson, 2007; Morton et al., 2007;
89 Switzer and Jones, 2008; Phantuwongraj and Choowong, 2012). Nonetheless,
90 criteria that have been used are still problematic and site specific or only valid for
91 known events (Gouramanis et al., 2014b). Many of these studies have relied on
92 sedimentological and stratigraphic signatures that can be found in both
93 tsunamigenic and cyclonic deposits. For example, Shanmugam (2012) reviewed 15

sedimentological criteria that had been found in both tsunami and storm deposits and drew the conclusion that “there are no reliable sedimentological criteria for distinguishing paleo-tsunami deposits in various environments” (p.23). Gouramanis et al. (2014b) used a multi-proxy approach (granulometric, loss on ignition, heavy minerals and microfossils) to statistically compare the 2004 IOT deposit and 2011 Cyclone Thane deposit superimposed at the same location along the southern coast of India. The Gouramanis et al. (2014b) study indicated that tsunami and storm deposits from the same site could not be distinguished using the standard sedimentological parameters typically used to identify coastal hazard deposits.

Thus, the difficulty of using conventional diagnostic criteria in differentiating coastal washover deposits requires the development of new and novel proxies.

In this study, we seek to test two hypotheses:

1. that the mineral composition, element geochemistry and grain size parameters of modern onshore, nearshore and offshore environments can be used to determine the provenance of the 2004 IOT and paleo-tsunami deposits, and the 2007 storm surge deposit preserved on Phra Thong Island, Thailand (Fig. 1); and
2. that the 2004 IOT, paleo-tsunami and the 2007 storm surge deposits can be distinguished using mineral composition, element geochemistry and grain size parameters.

To investigate these hypotheses, we apply several novel and seldom-used (for coastal hazard deposits) statistical techniques to gain insight into the provenance of the washover deposits and compare the deposits from different events and causal mechanisms (i.e. storm, recent and paleo-tsunami).

To date, little attention has focused on the mineralogy and geochemistry of overwash deposits (Chagué-Goff, 2010 and references therein). It is believed that the geochemical signature and mineral composition of tsunami sediments are source-dependent (Chagué-Goff et al., 2011; Goff et al., 2012), and are expected to reflect the origin of coastal overwash deposits (Font et al., 2013; Chagué-Goff et al., 2015). Addressing these issues will contribute a greater understanding of the sedimentation and hydrodynamic processes (i.e. erosion and deposition) occurring during coastal overwash sediment deposition (e.g. Switzer et al., 2012; Goff and Dominey-Howes, 2013; Sugawara et al., 2014).

2. Site description

Phra Thong Island is approximately 125 km north of Phuket on the west coast of southern Thailand in the Andaman Sea (Fig. 1). Phra Thong Island is characterized by a series of north-south trending, sandy Holocene beach ridges and marshy swales on the western side, and dense tidal mangroves on Pleistocene sand dunes on the eastern side (Jankaew et al., 2008; Brill et al., 2012a; Scheffers et al., 2012; Brill et al., 2015).

139 The offshore area is characterized by a shallow-gradient shelf dominated by quartz,
140 and minor carbonates (aragonite and calcite), feldspars (microcline, orthoclase,
141 labradorite), heavy minerals (cassiterite, zircon, garnet), muscovite, monazite and
142 kaolinite (Fig. 2 and Supp. Info Figs.S1-S2). The grainsize varies from medium- to
143 fine-sand in the nearshore and medium- to coarse-sand in water deeper than 15 m
144 (Fig. 2). This grain size distribution is similar to the offshore sediment grain size
145 described from offshore Pakarang Cape approximately 40 km south of Phra Thong
146 Island (Feldens et al., 2012). From the early 1900s to the 1970s and sporadically
147 since, tin and other heavy metals were mined both from the onshore and offshore
148 environments of Phra Thong Island (Jankaew et al., 2011). This activity would have
149 influenced the mineral phases transported onshore in the last 120 years.

150

151 During the 2004 IOT event, the maximum observed tsunami wave height was 20 m
152 - the highest recorded wave height along the Thai coast (Tsuji et al., 2006). More
153 importantly, on Phra Thong Island, the sedimentary signatures of the 2004 IOT and
154 at least three different past tsunami events (preserved as 5 to 20 cm thick sand
155 sheets in coastal swales) were identified by Jankaew et al. (2008).

156

157 Since Jankaew et al. (2008)'s study, the 2004 IOT tsunami and paleo-tsunami
158 deposits on Phra Thong Island have been extensively studied to determine the
159 chronology and potential tsunami recurrence interval (Fujino et al., 2009; Brill et
160 al., 2012a; Prendergast et al., 2012), micropaleontology (Sawai et al., 2009),
161 sedimentology and stratigraphy (Fujino et al., 2008; Fujino et al., 2009; Brill et al.,

2012a; Brill et al., 2012b; Brill et al., 2015), flow conditions (Choowong et al., 2008; Sawai et al., 2009; Brill et al., 2014) and a ground penetrating radar survey to image the thin tsunami beds (Gouramanis et al., 2014a; Gouramanis et al., 2015).

Phra Thong Island is rarely impacted by storms (Jankaew et al., 2008; Brill et al., 2014) but in early May 2007 an unusual tropical depression that formed in the upper part of Gulf of Thailand moved across southern Thailand (Thai Meteorological Department, 2007). As the tropical depression moved into the Andaman Sea, the depression interacted with the southwest monsoon resulting in heavy rain (200 to 400 mm) and intense onshore waves along the north-western coast of Thailand (Thai Meteorological Department, 2007). The resultant storm surge deposited sands upon the youngest berm of Phra Thong Island.

Although the shallow marine environment is considered to be the source of the sediments comprising the 2004 IOT deposit on Phra Thong Island based on evidence from diatom assemblages (Sawai et al., 2009) and grain size distribution (Fujino et al., 2008; Fujino et al., 2010), the provenance of the older deposits has not been identified. Thus, we aim to identify the provenance and compare the granulometry, mineralogy and geochemistry of the 2004 IOT tsunami, paleo-tsunami and 2007 storm deposits.

3. **Methods**

3.1. Sample collection

Sediment samples were collected in March 2012 and May 2013 from the offshore and nearshore marine environment, the modern beach and beach ridges inland, pits that contained the 2004 IOT and three palaeotsunami deposits (e.g., Jankaew et al., 2008), and pits through the 2007 storm deposit. Fourteen offshore samples were collected using a Van Veen grab from water depths ranging from 3 to 25 m and up to 10 km away from the modern shoreline. Eight onshore samples were collected from the modern beach and from 5 to 12 cm deep pits in locations where the 2004 IOT capped the ridges and swales. Four samples each of the 2004 IOT (Sand A) and the most recent prehistoric tsunami (Sand B) deposits were collected from a trench Swale Y (Jankaew et al., 2008). Three sediment samples of the third oldest palaeotsunami sandsheet (Sand C) was sampled from a pit 8.5 m south of the trench and two samples of the oldest palaeotsunami sandsheet (Sand D) from auger 10 (Fig. 1; Gouramanis et al., 2015).

3.2. Sediment analyses

Grain size analysis was performed at the Asian School of the Environment, Nanyang Technological University, Singapore, and X-ray diffraction (XRD) and X-Ray fluorescence (XRF) analyses were carried out at the X-ray laboratory, University of Wollongong, Australia.

3.2.1 Grain size analysis

Prior to grain size analysis, all of the sediment samples were treated in hydrochloric acid (HCl) to eliminate carbonate, and hydrogen peroxide (H_2O_2) to remove organic matter. The analysis of grain size parameters (i.e. mean, sorting, skewness and kurtosis) followed 60 s of ultrasonic dispersion, and grain size measured in triplicate using a Malvern Mastersizer 2000 (size range 0.02 μm to 2 mm). Granulometric parameters were obtained and described based on the logarithmic graphical method of Folk and Ward (1957) using the GRADISTAT package (Blott and Pye, 2001). The grain size was not measured for two offshore samples (PT-OS 07 and PT-OS 22) due to insufficient sample material and these two samples were excluded from further examination.

3.2.2 X-ray Diffraction (XRD)

The XRD analysis was conducted using a Philips PW 1771/00 diffractometer with Cu Kα radiation, X-tube at 1 kW and a Spellman DF3 generator (the angle of two theta ranged from 4 to 70˚, with a step size of 0.02˚). The raw XRD profiles derived from the diffractometer were analyzed using the TRACES 4.0 software. The corrected profiles were then processed in SIROQUANT software, which calculated the weight% (wt. %) of each mineral phase present (Williams et al., 2012).

Bulk mineral contents for the Deep-Offshore, Nearshore, Onshore, Sand A and Sand B samples were analysed using quantitative XRD. Unfortunately, the very high concentration of quartz (>80 wt. %) in the bulk analyses would dampen the

influence of the lower concentration minerals in the statistical analyses. Sand C, Sand D and 2007 Storm samples were not analysed but the dominance of quartz in these samples suggests a similar composition across the data set. So to investigate the role of the non-quartz component, the finer sediment fraction (63 to 125 μm) was analysed using XRD. The finer fraction XRD mineral composition was used in the statistical analyses.

3.2.3 X-ray Fluorescence (XRF)

Trace element contents were determined using a SPECTRO XEPOS energy dispersive polarization XRF spectrometer with a 50 Watt Pd end-window tube for excitation. It utilises a range of polarization and secondary targets to optimise excitation conditions for different elements. Samples for trace element analysis were prepared by pressing approximately 5 gm of powdered sample into an aluminium cup with a few drops of PVA binder and dried overnight at 70°C. Deconvolution of the spectra and conversion of X-ray intensities are performed using proprietary software developed by the manufacturer. Calibration of the instrument is made against a wide range of natural rock standards and synthetic materials.

3.3. Statistical methods

To determine the provenance of the sediments deposited by the 2004 IOT, paleo-tsunami and 2007 storm and to compare the overwash deposits, three multivariate statistical techniques (Partitioning Around Medoids (PAM), Principal Component

Analysis (PCA) and Discriminant Function Analysis (DFA)) were employed. Each technique was applied separately to grain size characteristics, mineral contents and trace element data. All statistical analyses were executed in *R* (R Core Team, 2014) by using the ***cluster*** (Maechler et al., 2014), ***vegan*** (Oksanen et al., 2016) and ***boot*** (Canty and Ripley, 2016) packages.

3.3.1. Partitioning Around Medoids - PAM

PAM is a type of cluster analysis that can be used to identify potential groups without prior knowledge of groups in a population (Kaufman and Rousseeuw, 2005). PAM chooses representative object(s) for group(s) from the data set and then forms cluster(s) by locating other objects to the predefined closest representative object (the medoids). The medoid minimises the sum of the Euclidean dissimilarity and clusters similar objects (Rousseeuw, 1987; Kaufman and Rousseeuw, 2005). The number of clusters (*k*) is defined *a-priori* to obtain the optimal *k* and PAM is run with *k* varying from 2 (smallest possible number of groups) to 8 (maximum number of groups) to compare the average silhouette widths and the largest average silhouette width value (Kaufman and Rousseeuw, 2005).

3.3.2. Principal Component Analysis – PCA

PCA simplifies multivariate data sets by transforming the original data to a new lower-dimensional (principal components) data set to simplify interpretations (Everitt and Hothorn, 2011). In addition, PCA can investigate the relationships between variables and the relationships among observations in a data set.

PCA was employed to study the interaction of all variables and the distribution of samples using granulometric data, mineralogy and geochemistry. All data sets were standardized prior to analysis and the correlation matrix was used to extract components due to different units and large variances in the data sets (Everitt and Hothorn, 2011). To retain the significant components from PCA analysis, the broken stick method and Kaiser-Guttman criteria applied was applied (e.g., Legendre and Legendre, 2012).

As the sample size (n = 36) and the number of variables (p) varies depending on the PCA performed ($p_{Grain\ size}$ = 4, $p_{Mineralogy}$ = 10 and $p_{Geochemistry}$ = 22), we test the significance, and hence stability, of each significant principal component (PC; (e.g., Jackson, 1993). To test for stability in each significant PC, the individual eigenvalues ($\hat{\lambda}$) were bootstrapped using an ordinary non-parametric bootstrap technique (e.g., Efron and Tibshirani, 1993) with 10,000 iterations and individual histograms investigated. Depending if the histogram resembles a normal-family distribution or skewed distribution, then the 95% confidence intervals on the resampled eigenvalues ($\hat{\lambda}$*) are calculated using the percentile or the bias-corrected methods (Efron and Tibshirani, 1993; Canty, 2002).

3.3.3. Discriminant Function Analysis - DFA

DFA is a classification technique that seeks the greatest separation between well-defined or known groups of a population using linear discriminant functions (Davis,

291 2002). Discriminant functions are linear combinations of a set of standardised
292 independent variables that create scores used to allocate group membership. DFA
293 concentrates on discriminating groups and the regression coefficients of the
294 discriminant functions maximize the ratio of between-group mean differences and
295 within-groups variance differences (Tabachnick and Fidell, 2013). The DFA
296 groupings were then graphically compared based on the *a priori* sedimentary
297 environment groupings.

298

4. Results

299 4.1. Analytical results

4.1.1. Grain size analysis

300 The Offshore group presents a wide range of grain size characteristics and can be
301 divided into two sub-groups: the Deep-Offshore group (>10m water depth; samples
302 include: PT-OS 03, PT-OS 05, PT-OS 13, PT-OS 15 and PT-OS 17) and the
303 Nearshore group (<10m water depth; samples include: PT-OS 24, PT-OS 26, PT-
304 OS 28, PT-OS 32, PT-OS 33, PT-OS 34; Fig. 1, Table 1).

305

306 The Deep-Offshore group is characterized by coarse to medium, poorly to
307 moderately sorted, very fine to finely skewed and mesokurtic to very leptokurtic
308 sand (Fig. 2, Table 1). The Nearshore group, in contrast, is composed of very fine to
309 fine, moderately to moderately well sorted, very finely skewed to symmetrical and
310 mesokurtic to very leptokurtic sand (Fig. 2, Table 1). Sample PT-OS 21, which lies

between the Deep-Offshore and the Nearshore group (Fig. 1), is characterized by very coarse very poorly sorted, finely skewed and leptokurtic silt (Fig. 2, Table 1).

The Onshore group consists of predominantly medium, moderately well sorted, symmetrical and mesokurtic sand, except PT-04, which is classified as a fine sand (Table 1). The Sand A and Sand B groups are very similar and composed of very fine, moderately to moderately well sorted, coarsely skewed to symmetrical and mesokurtic to leptokurtic sand (Table 1). The Sand C group is a fine, poorly sorted, finely skewed to symmetrical and very leptokurtic sand (Table 1). The Sand D and the Storm groups are both medium, moderately sorted to moderately well sorted, mesokurtic sands, but they differ slightly in skewness, with Sand D samples finely skewed and the Storm samples typically symmetrical (Table 1).

4.1.2. Mineralogy

The bulk sediment mineralogy suggests a relative homogeneity of the medium to coarse sands with quartz dominating (>80 wt. %) and minor aragonite, calcite and garnet being present. The fine sediment fraction mineralogy is still dominated by quartz (*ca*. 52 wt. % on average), though a range of other minerals are present including orthoclase, microcline, aragonite, zircon, cassiterite, monazite, kaolinite, muscovite and labradorite (Table 2). Calcite and garnet were not present in the finer fraction suggesting that these minerals are only present as coarse grains.The XRD results of the bulk sediment analyses show that quartz dominates the marine sediments with minor contributions of calcite, aragonite, zircon and garnet (Supp.

334 Info. Fig. S1). Notably, aragonite has high concentrations in the nearshore
335 environment south of the onshore sampling locations (~15 wt. %) and deeper
336 offshore (~12 wt. %) but persists in most samples at very low concentrations (Supp.
337 Info. Fig. S1).

For the fine mineralogical fractions, quartz dominates (>45 wt. %) the nearshore environment to depths of 15 to 20 m, but other minerals have locally high concentrations demonstrating the mineralogical heterogeneity of the marine environment in the northern part of Phra Thong Island (Fig. 2 and Supp. Info. Figs S2-S3). In the fine fraction, aragonite and muscovite are present throughout the marine environment but have locally high concentrations (aragonite: 12-15 wt. %, muscovite: 10 wt. %) in deeper environments (Supp. Info. Fig. S2). The northern nearshore environment and deep offshore environments contain high zircon (8 and 6 wt. %), orthoclase (16 wt. % in both environments) and microcline (9 and 12 wt. %), suggesting a similar mineral assemblage (Supp. Info. Fig. S3). Microcline also occurs in high concentrations in the nearshore zone south of the onshore sampling sites and between 10 and 20 m water depth to the north (Supp. Info. Fig. S3). Cassiterite, which has been extensively mined for tin (Jankaew et al., 2011), is found adjacent to the sampled overwash deposits in the nearshore environment (~1.5 wt. %) and in water depths ranging from 10 to 20 m (Supp. Info. Fig. S2).

4.1.3. Trace element geochemistry

The results from the 34 trace elements analysed show significant heterogeneity across the marine environment and in the onshore and overwash deposits (Fig. 2, Supp. Info. Figs S4-S6, Table 3). Several of the analysed elements are excluded from further discussion including:

- sulfur (S), chlorine (Cl) and bromine (Br) because they are typically marine elements with very high concentrations in the offshore samples and low in the other samples, and, therefore, they were likely to saturate the results;
- zinc (Zn), germanium (Ge), molybdenum (Mo), cadmium (Cd), antimony (Sb) and mercury (Hg) because they showed no variation between the groups and contribute little to dissimilarity tests; and,
- cobalt (Co), tantalum (T) and tungsten (W) because the high values of these elements were caused by contamination during the grinding process.

From this, 22 trace elements (V, Cr, Ni, Cu, As, Se, Rb, Sr, Zr, Nb, Sn, Ba, La, Ce, Hf, Pb, Th, U, Y, Cs, Ga, Bi) were included in the statistical analyses (Table 3).

Of these 22 trace elements, distinct elemental zones exist in the marine environment west of Phra Thong Island (Fig. 2 and Supp. Info. Figs S4-S6). Notably, the nearshore zone contains a high degree of trace element heterogeneity which mirrors the mineralogical heterogeneity.Immediately offshore from the onshore sampling sites the trace elements have high concentrations of Sr, Nb, Sn, La, Rb, Th, U, Y and Zr (Fig. 2 and Supp. Info. Fig. S4). Farther offshore in intermediate depth waters (10 to 20 m) As, Cr, Pb, V, Ba and Sr have high elemental concentrations (Fig. 2 and Supp. Info. Fig. S5). In the northern nearshore zone Ce, La, Th, U, Y and Zr have higher elemental concentrations than to the south, but also have high concentrations of Bi, Hf, Nb and Se (Fig. 2 and Supp. Info. Figs S4, S6). The nearshore environment south of the onshore sampling sites has high concentrations of Ba, Cr, Cu, Cs, Ga, Ni, Rb, Pb and V (Supp. Info. Figs S4-S6). The trace elemental concentrations in water deeper than 20 m have high Sr concentrations and, in the northern section, high Sn (Fig. 2).

384

385 4.2. Statistical results

386 In this section, the terms denoted by a subscript *GS*, *MIN* and *CHEM* are statistical
387 analyses (i.e. PAM, PCA and DFA) for the grain size parameters, mineral contents
388 and trace elements, respectively.

389

4.2.1 Grain size parameters

390 Four granulometric parameters (mean, sorting, skewness and kurtosis) were
391 examined using PAM_{GS}. The PAM_{GS} (Fig. 3) indicates that eight clusters can be
392 identified (overall average silhouette is 0.53). Cluster 1 includes one Sand A and
393 one Sand B sample (Fig. 3). Cluster 3 comprises all of Sand C and one Nearshore
394 sample. Cluster 4 incorporates most of the Sand A, Sand B (three samples for each
395 group) and four Nearshore samples (Fig. 3). Cluster 6 is composed of three Deep-
396 Offshore samples and all of Sand D samples. Cluster 7 is the largest cluster and is
397 made up of all of Onshore and Storm samples. Clusters 2, 5 and 8 contain only a
398 single sample for each group and their silhouette widths are zero (Fig. 3). The zero
399 silhouette width of these clusters implies a “neutral case” and samples in these
400 clusters can be also equally assigned to either neighboring cluster (e.g. the second-
401 best choice; Kaufman and Rousseeuw, 2005).

402

403 The PCA_{GS} result is consistent with the PAM_{GS} analysis (Fig. 4a). The broken stick
404 model (Fig. 4b) and Kaiser-Guttman criteria (Supp. Info Table S1) suggest that only
405 the first two principal components ($PC1_{GS}$ and $PC2_{GS}$) are necessary to explain 82%

406 of the variance in the grain size data set. The ordinary non-parametric bootstrap
407 analysis of $\hat{\lambda}^*$ does not differ significantly from the $\hat{\lambda}$ determined from the PCA for
408 either $PC1_{GS}$ or $PC2_{GS}$ indicating the stability of each principal component using the
409 available data. Histograms and quantile-quantile plots for $PC1_{GS}$ (Supp. Info. Fig.
410 S7) and $PC2_{GS}$ (Supp. Info. Fig. S7) demonstrate the relative normality of the
411 distributions of $\hat{\lambda}^*$, and that $\hat{\lambda}$ ($PC1_{GS}$ = 2.08 and $PC2_{GS}$ =1.206) resides within the
412 percentile 95% confidence interval of $\hat{\lambda}^*$ ($PC1_{GS}$ = (1.803, 2.616); and $PC2_{GS}$ =
413 (0.94, 1.395)).

414

415 $PC1_{GS}$ and $PC2_{GS}$ explain 52% and 30% of the variance, respectively. $PC1_{GS}$ is
416 defined by sorting, skewness and kurtosis and shows very little difference between
417 the Sand A, Sand B, Onshore and Storm deposits that overlap with the Nearshore
418 sediments (Fig. 4a). $PC1_{GS}$, also results in significant overlap between the grain size
419 parameters of the Nearshore, Deep Offshore, Sand C and Sand D (Fig. 4a). $PC2_{GS}$ is
420 defined by the mean sediment grain size and shows extensive overlap between each
421 of the overwash deposits and environments with the mean grain size of the Deep
422 Offshore environment (Fig. 4a). However, $PC2_{GS}$ does separate Sands A, B and C
423 that are situated within the Nearshore sediments, from the Storm deposits that are
424 very similar to the Onshore deposits (Fig. 4a).

425

426 Both $PC1_{GS}$ and $PC2_{GS}$ show a large scatter in the distribution of Deep-Offshore
427 and Nearshore sediments as seen in the Folk-Ward Classification (Table 1). In both
428 principal components, Sand A and Sand B samples, and the Onshore and Storm

429 samples overlap. There is a gradation in mean grain size from the Sand A and Sand
430 B samples to the Onshore and Storm samples with the Nearshore sediments
431 interspersed between these deposits. The Deep-Offshore sediments show a wide
432 distribution in $PC1_{GS}$ and $PC2_{GS}$ that reflects a high diversity of grain size
433 characteristics.

434

435 In the DFA_{GS}, discriminant function 1 ($DF1_{GS}$) is highly significant (percentage
436 separation is 75%) and separates Sand D and the Deep-Offshore groups from Sand
437 A, Sand B and most Nearshore samples (Fig. 5). Discriminant function 2 ($DF2_{GS}$;
438 accounts for 17% separation) discriminates Sand C from the remaining sediment
439 samples (Fig. 5). The similarity of Sand A and Sand B is demonstrated in the
440 DFA_{GS}, and these two groups are situated close to the three Nearshore samples (Fig.
441 5) as observed in the PCA_{GS} (Fig. 4a). The Storm and Onshore groups agree with
442 the PCA_{GS} results (Fig. 4a) and are defined by $DF2_{GS}$, which separates these
443 samples from Sand C.

444

4.2.2. Mineral content

445 Prior to the statistical analyses of the mineralogical data, we replaced the missing
446 value of muscovite in sample PT-OS 33 with the mean of muscovite contents in
447 samples from other Nearshore samples. Similarly, the mean of the labradorite
448 content for Onshore samples was substituted in sample PT-09.

449

The PAM_{MIN} determined only two clusters with an average silhouette width of 0.4. The first large cluster includes all of the Onshore, Sand A, Sand B and Nearshore samples and half of the Deep-Offshore group, while the second cluster comprises the rest of the Deep-Offshore group (Fig. 6).

The PCA_{MIN} result (Fig. 7a) is consistent with the PAM_{MIN} (Fig. 6) analysis showing a broad mineralogical transition from the Nearshore and Onshore deposits to the two most recent tsunami deposits (Sand A and Sand B). The broken stick model (Fig. 7d) and Kaiser-Guttman criteria (Supp. Info. Table 2) suggest that the first three principal components are necessary to explain most of the variance in the mineralogy data set. The first three principal components ($PC1_{MIN}$, $PC2_{MIN}$ and $PC3_{MIN}$) are sufficient to explain the mineralogy dataset and account for 81% of the explained variance (Fig. 7d and Supp. Info. Table 1).

The ordinary non-parametric bootstrap analysis of $\hat{\lambda}^*$ does not differ significantly from the $\hat{\lambda}$ determined from the PCA_{MIN} for either $PC1_{MIN}$, $PC2_{MIN}$ or $PC3_{MIN}$ indicating the stability of each principal component using the available data. Histograms and quantile-quantile plots for $PC1_{MIN}$ (Supp. Info. Fig. S8) and $PC2_{MIN}$ (Supp. Info. Fig. S8) are relatively normally distributions of $\hat{\lambda}^*$, and that $\hat{\lambda}$ ($PC1_{MIN}$ =3.58 and $PC2_{MIN}$ =2.69) resides within the percentile 95% confidence interval of $\hat{\lambda}^*$ ($PC1_{MIN}$ = (3.259, 4.98) and $PC2_{MIN}$ = (2.01, 3.31)). The histogram and quantile-quantile plot of $PC3_{MIN}$ (Supp. Info. Fig. S9) is skewed and a normal distribution

cannot be assumed. However, $\hat{\lambda}$ ($PC3_{MIN}$ =1.83) resides within the bias-corrected percentile 95% confidence interval of $\hat{\lambda}^*$ ($PC3_{MIN}$ = (1.27, 2.61).

$PC1_{MIN}$ (~36% of the variance) is only positively correlated with quartz content and is negatively correlated with labradorite, monazite, kaolinite and muscovite (Fig. 7a). Conversely, quartz does not significantly contribute to variations in $PC2_{MIN}$ (~27% of the variance) but zircon, orthoclase, microcline and cassiterite positively contribute to $PC2_{MIN}$. Labradorite, monazite, kaolinite and muscovite are also weakly negatively correlated with $PC2_{MIN}$ (Fig. 7a). $PC3_{MIN}$ (18% of the variance) is positively correlated with orthoclase, monazite and aragonite, and negatively correlated with muscovite, kaolinite, zircon and cassiterite when compared with $PC1_{MIN}$ (Fig. 7b). However, comparison between $PC2_{MIN}$ and $PC3_{MIN}$ (Fig. 7c) shows that orthoclase and aragonite are orthogonal to monazite, and muscovite and kaolin are orthogonal to zircon and cassiterite. Of note, aragonite appears to influence a single Deep Offshore sample and a single Sand B sample, likely due to the presence of coral rubble, which is not present in any other sample.

The first three principal components show that Sand A and Sand B are mineralogically indistinguishable (Fig. 7a-c) and that most of the Nearshore and Onshore sediments cluster around the origin of the three principal component plots highlighting the relative mineralogical homogeneity (Fig. 7a-c). Even after the removal of coarse-grained quartz, the Nearshore samples are influenced by increasing concentrations of fine-grained quartz, whereas the Onshore sediments

have relative higher concentrations of zircon, orthoclase, microcline and cassiterite (Fig. 7a-c). The Deep Offshore samples have elevated labradorite, muscovite, monazite and kaolinite concentrations relative to other minerals (Fig. 7a-c).

The DFA_{MIN} shows that the Deep-Offshore group is distinct and dispersed from other groups, especially along the $DF2_{MIN}$ (Fig. 8). $DF1_{MIN}$ (52% of the separation) discriminates the Deep-Offshore, Nearshore and Sand A from Sand B and Onshore group very well (Fig. 8). In contrast, $DF2_{MIN}$ (39% of the separation) only separates Sand A group from Sand B samples, but that these two deposits overlap with the Nearshore and Onshore sediments (Fig. 8). Combined, both $DF1_{MIN}$ and $DF2_{MIN}$ show that Sand A sediments are mineralogically similar to the Nearshore sediments, and that Sand B and the Onshore sediments have a similar mineralogy (Fig. 8).

4.2.3. Trace elements

Twenty-two trace elements were used to investigate the relationship between the environments and overwash deposits using PAM, PCA and DFA analyses. Prior to PAM , PCA and DFA analyses of the geochemistry data, three samples (one Sand D and two Onshore samples) were removed due to their very high Zr concentrations that heavily influenced the analysis (not shown).

The PAM_{CHEM} analysis identified two clusters (average silhouette width of 0.36). The first cluster contained all of the Sand B samples, one Nearshore sample, one Deep-Offshore and one Sand D sample (Fig. 9). Based upon the PAM_{CHEM} analysis

518 the two latter samples are misclassified, suggesting that these two samples would
519 have been assigned to the second cluster (i.e. the second best choice, e.g. Kaufman
520 and Rousseeuw (2005). The large second cluster comprises all of the remaining
521 samples (Fig. 9) indicating a similarity in the chemical composition between the
522 Onshore, Sand A, Sand C, Sand D, Nearshore and Storm samples.

523

524 The first two principal components of the PCA_{CHEM} are shown in Figure 10a,
525 although the broken stick model (Fig. 10d) suggests that four principal components
526 are necessary to explain the variance in the geochemistry data. The Kaiser-Guttman
527 criteria (Supp. Info. Table 3) suggest that the first five principal components
528 ($PC1_{CHEM}$ = 37%, $PC2_{CHEM}$ = 27%, $PC3_{CHEM}$ = 10%, $PC4_{CHEM}$ = 9% and $PC5_{CHEM}$ =
529 5%) are necessary to explain the variance in the geochemistry data set (88%).
530 $PC3_{CHEM}$ and $PC4_{CHEM}$ are very close to the cut-off for significance and $PC5_{CHEM}$ is
531 well below the broken stick cut-off. Thus, for the simplicity of interpretation,
532 $PC3_{CHEM}$, $PC4_{CHEM}$ and $PC5_{CHEM}$ are not discussed further.

533

534 As with the grain size and mineralogical data, the ordinary non-parametric
535 bootstrap analysis of $\hat{\lambda}^*$ does not differ significantly from the $\hat{\lambda}$ determined from the
536 PCA_{CHEM} for either $PC1_{CHEM}$ or $PC2_{CHEM}$ indicating the stability of each principal
537 component using the available data. Histograms and quantile-quantile plots for
538 $PC1_{CHEM}$ (Supp. Info. Fig. S10) and $PC2_{CHEM}$ (Supp. Info. Fig. S10) are skewed and
539 a normal distribution cannot be assumed. However, $\hat{\lambda}$ ($PC1_{CHEM}$ = 8.23 and

$PC2_{CHEM}$ = 5.95) resides within the bias-corrected percentile 95% confidence interval of $\hat{\lambda}^*$ ($PC1_{CHEM}$ = (7.23, 9.46) and $PC2_{CHEM}$ = (3.79, 7.62)).

The $PC1_{CHEM}$ shows positive correlations with Sand B, Sand D and most of the Nearshore samples (Fig. 10a), whereas most of the Deep-Offshore, Onshore and all of the Sand C and Storm sediments are negatively correlated to $PC1_{CHEM}$ (Fig. 10a). $PC1_{CHEM}$ is positively correlated with a cluster of variables including La, Ce, Th, Zr, Y, U and Hf. This cluster strongly drives variations along the $PC1_{CHEM}$ and thus separates Sand B from the other groups (Fig. 10a). The Deep Offshore, Onshore, Sand C and the Storm deposits are depleted in all of the analysed elements (Fig. 10a). $PC2_{CHEM}$ is characterized by strong positive correlations with As, V and Sr that separate two of the Deep offshore samples from the other samples (Fig. 10a), and negative correlations with Nb, Sn. Nb and Sn that are only found in high concentrations in Sand D (Fig. 10a).

$PC1_{CHEM}$ and $PC2_{CHEM}$ show that most of the sediment samples cluster around the origin of the axes (i.e. from -1 to 1 standard deviation), and only two Deep Offshore samples, one Nearshore sample, Sand B and Sand D contribute most of the variation in the PCA_{CHEM}. The PCA_{CHEM} shows that many of the elements are highly correlated suggesting that many elements can be excluded from the DFA, but still explain most of the variance of the data set. Here, elements that have high correlation coefficients (i.e. $r \geq 0.9$) with other elements were eliminated to avoid significant loss of information. Thus, from the cluster of highly correlated variables

La, Ce, Y, Hf, Zr, U and Th (Supp. Info. Table S4), La, Ce and Y were excluded as they are rare earth elements and are less reliably determined when analyzed by XRF. Hf was also eliminated due to a smaller loading value (0.86) in $PCA1_{CHEM}$ compared to U (0.9) and Th (0.94). Zr was retained since this element has been attributed to high-energy environments (Chagué-Goff et al., 2011) and is present in high concentrations in zircon.

Rb is also highly correlated with Ba (r = 0.94, Supp. Info. Table S4) but Ba was selected because it occurs in carbonate minerals. Similarly, the correlation coefficient between Sn and Nb is very high, r = 0.98, but Sn was used in DFA_{CHEM} because it is associated with cassiterite and is important to the island's historical mining activities.

The results of the DFA_{CHEM} analysis show that the first two discriminant functions highlight a complex arrangement of each environment and sediment group's relationship to the other groups (Fig. 11). $DFA1_{CHEM}$ accounts for 32% of the separation and is a gradation between three pairs of indistinguishable and overlapping groups: Sand C-Storm, Nearshore-Sand B and Sand A-Onshore (Fig. 11). The $DFA1_{CHEM}$ separates the three pairs of groups and also discriminates the Deep-Offshore group. Sand D has one sample overlapping with the Nearshore-Sand B and another sample located close to the Sand C-Storm groups along $DFA1_{CHEM}$ (Fig. 11).

585 $DFA2_{CHEM}$ (24% of the separation) cannot separate the Deep-Offshore from the
586 Nearshore group and there is a little overlap in their scores with the Sand C group's
587 score (Fig. 11). These three groups are well discriminated from the Storm, Sand A
588 and Onshore group in which the Storm and Sand A are almost identical. The
589 $DFA2_{CHEM}$ also discriminates Sand B and Sand D from other groups (Fig. 11).

590

5. Discussion

591 5.1. Proxies and impact factors in the study site

5.1.1. Geochemical signatures

592 The use of sediment geochemistry as a tool for studying coastal overwash deposits
593 is still in its early stages even though an increasing number of studies have utilized
594 geochemical signatures (see Chagué-Goff, 2010 for a review). For example,
595 Chagué-Goff et al. (2012a) traced the maximum inundation of the 2011 Tohoku-oki
596 event by using marine-derived salts in mud deposits (i.e. S and Cl) and suggested
597 these as potential identifiers for paleo-tsunamis. Font et al. (2013) combined
598 geochemical signatures with other proxies to identify the sediment source of the
599 1755 Lisbon tsunami deposits. Geochemical signatures (e.g. water-soluble salts and
600 metalloids) also have been used for environment impact assessments in the short
601 time after tsunami events in both tropical settings (e.g. Szczuciński et al., 2005) and
602 temperate environments (e.g.Chagué-Goff et al., 2012b).

603

604 The major challenge comes from the impact of post-depositional changes (e.g.
605 dilution or weathering processes) that may alter the concentration of elements after

606 events have occurred (Szczuciński et al., 2007; Chagué-Goff, 2010; Shanmugam,
607 2012; Font et al., 2013). For instance, a cyclone-related event normally causes
608 heavy rainfall that can quickly dilute concentration of marine salts in storm deposits
609 and therefore might bias the interpretation. Similarly, Szczuciński et al. (2007) also
610 reported a major decrease of water-soluble salts in the 2004 tsunami deposits due to
611 rainy season in several locations in Thailand, south of Phra Thong Island. These
612 studies reveal that saltwater signatures (i.e. salt) are very sensitive to environmental
613 changes (e.g. dilution or leaching processes). And as Phra Thong Island is also
614 affected by heavy precipitation (the rainy season is from April to November with
615 approximately 1900 mm of rainfall, based on the 1971-2000 data period (Thai
616 Meteorological Department (2012), that causes significant vertical movement of the
617 fresh watertable resulting in remobilization of the marine-derived salts in both
618 tsunami and storm deposits. Szczuciński et al. (2007) concluded that other
619 elements, such as heavy metals and metalloids, were not affected by rainfall and
620 therefore could be used to study the provenance of sediments deposited during
621 tsunami inundation (e.g. Chile; Chagué-Goff et al., 2015). Thus, taking that into
622 account, the present study focused on using a wide range of metalloid and heavy
623 metals.

624

625 In the modern marine environment trace elements vary spatially and can provide
626 insights into the sediment source of coastal overwash deposits. Understanding the
627 depth at which elements and minerals are concentrated in the modern environment
628 may shed light on the depth at which the elements and minerals were mobilized
629 prior to deposition as overwash deposits. This is akin to the analysis of microfauna

and microflora to determine depths of scour during coastal overwash (e.g. Tanaka et al., 2012).

5.1.2. Grain size parameters

Granulometric characteristics can provide useful information about sediment origin, sedimentation and hydrodynamic processes and have been extensively used in comparing tsunami and storm deposits (e.g. Nanayama et al., 2000; Goff et al., 2004; Tuttle et al., 2004; Kortekaas and Dawson, 2007; Morton et al., 2007; Gouramanis et al., 2014b) or in interpreting tsunami or storm events (e.g., Switzer and Jones, 2008).

The spatial distribution of mean grain size from offshore Phra Thong Island shows that the shallow marine samples are generally finer than those from deeper water (Fig. 2.2). In addition, the mean grain size and selected trace elements are highly positively correlated (Supp. Info. Table S2.5). This correlation reflects that most trace elements are found in heavy minerals that are finer and possibly concentrated nearshore over time.

In regard to temporal variability, Szczuciński et al. (2007) reported the effect of rainfall on the mean grain size of the 2004 IOT deposits after one year and found a coarsening in half of the sandy tsunami samples. This change was ascribed to heavy rain that had removed the finer fraction from sandy tsunami deposits during the rainy season and, therefore, the effect of rainfall over time should be taken into

account in paleo-tsunami studies in tropical climates (e.g. Thailand; Szczuciński et al., 2007). In contrast to tropical regions, fine-grained deposits are more likely to be eroded quickly by aeolian forces in arid regions (e.g. Peru; Spiske et al., 2013).

5.1.3. Mineral contents

Mineral compositions have recently been used as a useful tool (mostly with the focus on heavy mineral assemblages) in washover deposit studies (e.g. Switzer et al., 2005; Szczuciński et al., 2005; Szczuciński et al., 2006; Jagodziński et al., 2009; Jagodziński et al., 2012; Switzer et al., 2012; Cuven et al., 2013; Font et al., 2013; Gouramanis et al., 2014b). The mineral content of the bulk samples from Phra Thong Island is dominated by quartz (>80 wt %). This result is consistent with mineral compositions reported by Jankaew et al. (2011) who noted a very high concentration of quartz (*ca*. 85 to 90 wt %) and a very small concentration of heavy minerals (*ca*. 1.7 to 2 wt % mostly of small cassiterite grains) in both the 2004 IOT deposits and paleo-tsunamis deposits on Phra Thong Island.

Our analytical analysis of the finer sand fraction (0.063 to 0.125 mm) considerably reduced the concentration of quartz and more minor minerals were detected implying that the finer sediment mineralogical fraction provides more meaningful information on the mineralogical variability of the overwash deposits. Unfortunately, due to the coarse grain size of Sand C, Sand D and the Storm samples, insufficient material prevented mineral analysis of these fine fractions. This difficulty prevented contrasting the older tsunami deposits and the storm

674 deposit, but with the dominance of quartz across our sample set, we suggest that the
675 use of mineral composition in this case is unlikely to be useful. Likewise,
676 Jagodziński et al. (2012) could not use heavy mineral assemblages as a proxy to
677 distinguish Tohoku-oki tsunami deposits from onshore sediments but noted that the
678 result might differ when using a smaller size fraction (e.g. mud fraction). Similarly,
679 Gouramanis et al. (2014b) also highlighted the difficulty of using heavy minerals in
680 conjunction with key grain size parameters to discriminate tsunami and storm
681 deposits due to the significant variations between and within pits on the southern
682 Indian coastline.

683

684 5.2. Implications for studying coastal overwash deposits

5.2.1. Discrimination of modern tsunami and storm deposits

685 Due to a lack of mineral content data for the storm deposit and oldest paleo-tsunami
686 deposits, we only use the statistical results from the elemental concentrations and
687 granulometric parameters to investigate whether the Storm and Sand A can be
688 discriminated.

689

690 In the PAM_{CHEM} (Fig. 9), our results show that both the Sand A deposits and those
691 of the 2007 Storm cannot be discriminated using geochemistry. This result implies
692 that the Storm and Sand A deposits are likely composed of the same minerals, the
693 geochemical data are inadequate for distinguishing the two deposits and that the
694 mechanism in which the sediments were deposited cannot be defined (Fig. 9).

695

696 The PCA_{CHEM} shows that the Sand A deposit is similar to the Storm deposit but that
697 these deposits cluster around the origin of the two first principal components
698 (within 1 standard deviation; Fig. 10) suggesting that none of the trace metals
699 contribute significantly to discriminating the two deposits. However, the DF_{CHEM}
700 discriminates Sand A from the Storm deposit due to the subtle loadings of each
701 trace element (most likely Sr, As and V) on $DF1_{CHEM}$ (Fig. 11). The granulometric
702 data (PAM_{GS}, PCA_{GS}, DFA_{GS}) suggest that the 2007 Storm and Sand A deposits can
703 be discriminated. In the PAM_{GS}, these two groups occur in different clusters (Fig. 3)
704 indicating a significant difference in grain size parameters between the two recent
705 overwash deposits. The PCA_{GS} reveals that the mean grain size is the only key
706 feature to distinguish the 2007 Storm deposits (medium sand) from those of the
707 Sand A (very fine sand; Fig.2. 4 and Table 2.1). This result is mirrored in the
708 DFA_{GS} analysis (Fig. 5). The results of other granulometric parameters (sorting,
709 skewness and kurtosis) show very little difference between the deposits of the
710 Storm and Sand A.

5.2.2. Provenance of the tsunami deposits

711 *Sand A*

712 The results for trace element (PCA_{CHEM}), mineralogy (PCA_{MIN}, DFA_{MIN}) and grain
713 size (PAM_{GS}, PCA_{GS} and DFA_{GS}) analyses suggest that most of the Sand A deposit
714 is predominantly derived from the shallow nearshore environment, although some
715 contribution from onshore beach sediment cannot be discounted (e.g. DFA_{CHEM}).
716 This conclusion agrees with Sawai et al.'s (2009) examination of the diatoms
717 preserved in Sand A on Phra Thong Island from the same sites examined here, and
718 Jagodziński et al. (2009) who suggested that the heavy mineral suite of the seafloor

sediments, beach sediment and local soils combined to form the tsunami deposits on Kho Khao Island (~20 km south of Phra Thong Island).

Paleo-tsunami

While the provenance of Sand A deposits has been identified, the provenance of prehistoric tsunami deposits is less clear. Our statistical results show that all three paleo-tsunami deposits differ from each other and the Sand A deposit, and thus suggest variable sources of the paleo-tsunami sediments or potential diagenetic alteration.

The grain size, mineralogical and trace element analysis of Sand B presents a complex history. The grain size analysis (PAM_{GS}, PCA_{GS}, and DFA_{GS}) indicates a strong similarity to Sand A and is closely related to the Nearshore sediments. Mineralogically, Sand B and Sand A are very similar in (PAM_{MIN} and PCA_{MIN}) with overlap with the Nearshore sediment mineralogy. However, DFA_{MIN} suggests that Sand B is closely related to the Onshore sediments. Geochemically, Sand B contains high concentrations of Th, Ce, La, Y and U similar to the Nearshore (PCA_{CHEM}) and these elements define $DF1_{CHEM}$. Thus Sand B is very likely a mixture of Onshore and Nearshore sediments.

Prendergast et al. (2012) beach ridge plain evolution model suggested that the formation of a new beach ridge complex occurs every 500 years, so Sand B, which was deposited between *ca*. 350 to 430 years ago (from optically stimulated

742 luminescence (OSL), Prendergast et al., 2012) and *ca.* 550-700 years ago (from 14C
743 Accelerator Mass Spectrometry, Jankaew et al., 2008) may have been affected by
744 the presence of a new beach ridge. However, the significant difference in the trace
745 metal composition between Sand B and Sand A deposits may indicate that either
746 post-depositional processes could have modified the deposit and/or the offshore
747 sediment geochemistry has been strongly modified since Sand B was deposited.

748

749 The interpretations of the provenance of the Sand C and Sand D deposits are also
750 complex. The grain size (PAM_{GS}, PCA_{GS} and DFA_{GS}) and geochemical (PAM_{CHEM},
751 PCA_{CHEM} and DFA_{CHEM}) analyses demonstrate that these two tsunami deposits
752 differ substantially from each other and Sands A and B. PCA_{GS} and DFA_{GS} analyses
753 show Sand D is similar to the Deep-Offshore sediments, while Sand C differs
754 significantly from all of the other groups (Figs 4 and 5). The PCA_{CHEM} shows that
755 Sand D is geochemically dissimilar to the other tsunami and storm deposits (Fig.
756 10), but Sand D shares similarities with Sand B in the DFA_{CHEM} (Fig. 11). For Sand
757 C, multivariate techniques reveal that both Sand C and the Storm group appear to be
758 similar in their geochemical composition (Figs 10 and 11).

759

760 This suggests that Sand C and Sand D were possibly derived from sediment sources
761 different from Sand A and Sand B. Nevertheless, the complexity of results and the
762 lack of historical and geological evidence prevent us from determining exactly
763 where the deposits originated. For example, the similarity of Sand C and the Storm
764 deposits in their geochemistry might lead to a suggestion that Sand C was deposited

765 by a paleo-storm and not by a paleo-tsunami (c.f. Jankaew et al., 2008). However,
766 Sand C is the thickest and most far-ranging paleo-overwash deposit preserved on
767 Phra Thong Island, and Phra Thong Island is not impacted by storms capable of
768 distributing sediments on this scale due to its geographical setting (Jankaew et al.,
769 2008). Thus, the use of geochemical information in deriving a cause for such
770 deposits is difficult to reconcile. In such cases, the term “large marine overwash
771 event” proposed by Switzer et al. (2014) should be used when the causes and
772 provenance remain unknown.

773

5.2.3. Provenance of the storm deposit

774 The provenance of the Storm deposit is most likely from the onshore sediments
775 preserved on the modern beach and beach berm based on the grain size (PAM_{GS},
776 PCA_{GS}, and DFA_{GS}) and trace element (PCA_{CHEM}) analysis. The DFA_{CHEM} analysis
777 indicates separation of the Storm and Onshore deposits, but that the Storm deposits
778 are very similar to the Sand C deposits.

779

5.2.4. Temporal geochemical variations – insights into post-depositional changes

780 It is important to study the temporal variations of elemental concentrations in order
781 to understand the impacts of post-depositional changes and to validate the
782 usefulness of sediment chemistry in paleo-tsunami deposits. However, only a few
783 publications have investigated how tsunami deposits have become geochemically
784 altered across different time scales and climate regions (e.g. Szczuciński et al.,
785 2006; Szczuciński et al., 2007; Chagué-Goff et al., 2012a; Chagué-Goff et al.,

2012b). Geological evidence on Phra Thong Island offers a unique opportunity to compare the modern tsunami deposits with three other paleo-tsunamis that, in turn, could provide more detail on geochemical signatures with more elements compared to previous works.

The concentration of 22 trace elements that have significant variations were plotted to compare between all of the tsunami deposits (Fig. 12). The results show that there is no consistent variability in the different tsunami deposits. In general, the trace elements can be divided into three sub-groups that have the same trends based on the elements' relative concentrations in each tsunami deposit. The first sub-group includes Sr, V and Cu that have high or very high concentrations in Sand A but are low or very low in the older tsunami deposits (Fig. 12); the second sub-group consists of elements that have the highest concentration in Sand B (Ni, La, Ce, Pb, Th, U, Y, Ba and Rb; Fig. 12); and, the third sub-group consist of elements that have the highest value in Sand D (Zr, Nb, Sn and Hf; Fig. 12). In two-thirds of the elements, Sand C deposits contain the lowest concentrations compared to the other three tsunami deposits (Fig. 12).

All observations in Sand A and paleo-tsunami deposits reveal that there is no simple trend in the temporal variation of the trace element chemistry on Phra Thong Island. This complexity might not be fully explained due to the lack of knowledge about how heavy-metal elements spatially vary in the marine system over time. In addition, local settings and depositional environment also play an important role in

809 chemical alterations (Chagué-Goff et al., 2011). For example, based on the
810 variations of Sr in our data set, we observe that Sr concentration is much higher in
811 the modern deposits and very low in the three other prehistoric tsunami deposits
812 (Fig. 12). The low Sr concentration in the deeper and older sand layers possibly
813 corresponds to the lack of inorganic and biogenic carbonate microfossils in the
814 deposits, which are rapidly dissolved due to elevated ambient temperatures and high
815 volumes of precipitation causing significant groundwater fluctuation through acidic
816 peat-rich environments (Jankaew et al., 2008; Sawai et al., 2009). In contrast to our
817 results, Chagué-Goff et al. (2012a) reported very little difference in Sr
818 concentration between the 2011 Tohoku-oki tsunami deposits and the 869 A.D.
819 Jogan tsunami deposits in Japan highlighting the site-specific feature of
820 geochemical signatures.

821

822 The evidence presented here from Phra Thong Island raises questions about the
823 reliability of using geochemical signatures for studying paleo-tsunami deposits (e.g.
824 sediment provenance). Therefore, there is a concern with the recent study of
825 Kuwatani et al. (2014) in which a set of chemical elements was proposed that could
826 be used to identify tsunami deposits from surrounding sediments. The method used
827 in this study suggested that elements such as Na, Ca and Mg could be useful in
828 discriminating tsunami deposits from other sediments, but this study lacks
829 validation using the paleo-tsunami deposits. Ca and Sr have very similar chemical
830 behaviour and our data show that Sr is strongly depleted in prehistoric deposits in
831 Thailand (Fig. 12). Similarly, other metals that are easily transported as salts and
832 carbonates (i.e. Na and Mg) also can be very quickly remobilized in short time

833 periods. Kuwatani et al. (2014) also proposed other heavy metal elements (e.g. Cr,
834 Cu, Pb) are useful to identify tsunami deposits, but our data show that these
835 elements vary considerably between overwash deposits recorded at the same site.
836 Hence, there is no guarantee that this set of elements can be widely applied.

837

5.2.5. Comparison of the statistical analyses

838 The use of three different statistical techniques allows us to compare between the
839 techniques.

840

841 PAM analysis is based on simple Euclidean distance to assign samples, but both
842 PCA and DFA have to solve more complicated matrices within and between
843 groups. Our PAM results showed significant differences in the environments and
844 overwash deposits with eight groups identified when the grain size parameters were
845 examined. However, for the mineralogy and geochemistry, there was insufficient
846 separation between the deposits and environments and in each case only two groups
847 with samples from multiple environments and deposits were recognized. The
848 mineralogical and geochemical analyses using PAM therefore were of little use in
849 discriminating the deposits and identifying the provenance of the sediments in each
850 deposit.

851

852 The PCA analysis proved to be a significant improvement on gaining insight into
853 the complexity and inter-relationship between each of the grain size, mineralogical
854 and geochemical parameters investigated. Applying bootstrap analysis to the

855 eigenvalues to test for stability in the derivation of principal components has not
856 been applied previously in coastal hazard studies and is a necessary step in
857 evaluating the significance of each principal component. Achieving stability in the
858 principal components indicates that the principal components derived from the data
859 are not significantly different from random resampling of the data. This validation
860 of the principal components demonstrates that the sample size used in each PCA is
861 sufficient to provide meaningful and accurate results on the relationship between
862 parameters and sampling sites.

863

864 The results of the DFA analysis differed from the PCA analysis and were expected
865 to do so. The PCA analysis seeks to define axes which maximize the variance of
866 each variable to compare variables and individual samples in multivariate space,
867 whereas the DFA seeks to identify a model of all of the variables to extract the
868 maximum separation in multidimensional space. Thus the two methods can be used
869 simultaneously and different information gleaned. Where the two methods agree
870 further credence is added to identifying the provenance of overwash deposits or
871 comparing between deposits. Where the two methods disagree, both methods can
872 provide valuable insight into the nature of the sedimentary deposits.

873

6. Conclusions

874 In this study, we examined the use of grain size parameters, mineral composition
875 and trace element geochemistry in determining the provenance of tsunami (the 2004
876 IOT and three paleo-tsunami) deposits and the 2007 storm surge deposit on Phra

877 Thong Island, Thailand. We also evaluated whether the 2004 tsunami and 2007
878 storm deposits could be discriminated using grain size and geochemistry. Our
879 statistical analyses, including cluster analysis, PCA and DFA, suggest that the two
880 modern washover deposits are geochemically indistinguishable whereas the mean
881 grain size of the sediment appears to be the only good discriminator of the storm
882 and the 2004 tsunami deposits. Therefore, the trace element composition cannot be
883 used as diagnostic criteria to distinguish known tsunami and storm deposits from
884 Phra Thong Island. If known storm and tsunami deposits cannot be distinguished
885 using these criteria, can these criteria be used to distinguish unknown or
886 hypothesised overwash processes?

887

888 Regarding the provenance of coastal overwash deposits, our statistical results
889 reaffirm that the 2004 IOT deposits were mainly generated from the shallow
890 nearshore environment, which is consistent with previous studies. Meanwhile, the
891 provenance of palaeotsunami deposits is rather complicated and might not be fully
892 explained by the data sets used in this study. Sand B is very likely a mixture of
893 onshore and nearshore sediments but the sources of Sand C and Sand D are unclear.
894 The difficulty in accurately identifying the provenance of the palaeotsunami
895 deposits is probably compounded by past long-term offshore mining activities (for
896 Sand B) and/or diagenetic alteration (for Sand C and Sand D). Thus, our findings
897 cast doubt on the utility of performing sediment chemistry to discriminate overwash
898 deposits, and to characterize the sediment source and source environment of
899 overwash sediments. However, the statistics-based approach in this study is capable

of providing meaningful insights into studies of coastal overwash deposits and shows promise for other locations where overwash deposits are preserved.

Acknowledgements

This research is supported by National Research Foundation Singapore (National Research Fellow Award No. NRF-RF2010-04) and the Singapore Ministry of Education under the Research Centres of Excellence initiative. KJ thanks A1B1-2 grant (RES-A1B1-34) from the Faculty of Science, Chulalongkorn University for financial support to collect storm deposit samples. We thank Joshua Kartik for the finer fraction assistance, Ronnakrit Rattanasriampaipong for fieldwork assistance and Chuoi Tongjin for his hospitality. This work comprises Earth Observatory of Singapore contribution No. 88.

REFERENCES

Blott, S.J., Pye, K., 2001. Gradistat: A grain size distribution and statistics package for the analysis of unconsolidated sediments. Earth Surface Processes and Landforms 26, 1237-1248.

Brill, D., Jankaew, K., Brückner, H., 2015. Holocene evolution of Phra Thong's beach-ridge plain (Thailand) — Chronology, processes and driving factors. Geomorphology 245, 117-134.

Brill, D., Klasen, N., Brückner, H., Jankaew, K., Scheffers, A., Kelletat, D., Scheffers, S., 2012a. OSL dating of tsunami deposits from Phra Thong Island, Thailand. Quaternary Geochronology 10, 224-229.

Brill, D., Klasen, N., Jankaew, K., Brückner, H., Kelletat, D., Scheffers, A., Scheffers, S., 2012b. Local inundation distances and regional tsunami recurrence in the Indian Ocean inferred from luminescence dating of sandy deposits in Thailand. Natural Hazards and Earth System Sciences 12, 2177-2192.

Brill, D., Pint, A., Jankaew, K., Frenzel, P., Schwarzer, K., Vött, A., Brückner, H., 2014. Sediment Transport and Hydrodynamic Parameters of Tsunami Waves Recorded in Onshore Geoarchives. Journal of Coastal Research 297, 922-941.

Canty, A., 2002. Resampling Methods in R: The boot Package. R News 2(3), 2-7.

Canty, A., Ripley, B., 2016. Boot: Bootstrap R (S-Plus) Functions. R package version 1.3-18. https://cran.r-project.org/web/packages/boot/index.html

Chagué-Goff, C., 2010. Chemical signatures of palaeotsunamis: a forgotten proxy? Marine Geology 271, 67-71.

Chagué-Goff, C., Andrew, A., Szczuciński, W., Goff, J., Nishimura, Y., 2012a. Geochemical signatures up to the maximum inundation of the 2011 Tohoku-oki tsunami - implications for the 869AD Jogan and other palaeotsunamis. Sedimentary Geology 282, 65-77.

Chagué-Goff, C., Goff, J., Wong, H.K.Y., Cisternas, M., 2015. Insights from geochemistry and diatoms to characterise a tsunami's deposit and maximum inundation limit. Marine Geology 359, 22-34.

Chagué-Goff, C., Niedzielski, P., Wong, H.K.Y., Szczuciński, W., Sugawara, D., Goff, J., 2012b. Environmental impact assessment of the 2011 Tohoku-oki tsunami on the Sendai Plain. Sedimentary Geology 282, 175-187.

Chagué-Goff, C., Schneider, J.L., Goff, J.R., Dominey-Howes, D., Strotz, L., 2011. Expanding the proxy toolkit to help identify past events - lessons from the 2004 Indian Ocean Tsunami and the 2009 South Pacific Tsunami. Earth-Science Reviews 107, 107-122.

Choowong, M., Murakoshi, N., Hisada, K., Charoentitirat, T., Charusiri, P., Phantuwongraj, S., Wongkok, P., Choowong, A., Subsayjun, R., Chutakositkanon, V., Jankaew, K., Kanjanapayont, P., 2008. Flow conditions of the 2004 Indian Ocean tsunami in Thailand, inferred from capping bedforms and sedimentary structures. Terra Nova 20, 141-149.

Cuven, S., Paris, R., Falvard, S., Miot-Noirault, E., Benbakkar, M., Schneider, J.L., Billy, I., 2013. High-resolution analysis of a tsunami deposit: case-study from the 1755 Lisbon tsunami in southwestern Spain. Marine Geology 337, 98-111.

Davis, J.C., 2002. Statistics and Data Analysis in Geology third ed. John Wiley & Sons, New York.

Efron, B., Tibshirani, R., 1993. An introduction to the bootstrap. New York : Chapman & Hall, c1993.

Everitt, B., Hothorn, T., 2011. An Introduction to Applied Multivariate Analysis with R: Use R! Springer, New York.

Feldens, P., Schwarzer, K., Sakuna, D., Szczuciński, W., Sompongchaiyakul, P., 2012. Sediment distribution on the inner continental shelf off Khao Lak (Thailand) after the 2004 Indian Ocean tsunami. Earth, planets and space 64, 875-887.

Folk, R.L., Ward, W.C., 1957. Brazos River bar [Texas]; a study in the significance of grain size parameters. Journal of Sedimentary Research 27, 3-26.

Font, E., Veiga-Pires, C., Pozo, M., Nave, S., Costas, S., Ruiz Muñoz, F., Abad, M., Simões, N., Duarte, S., Rodríguez-Vidal, J., 2013. Benchmarks and sediment source(s) of the 1755 Lisbon tsunami deposit at Boca do Rio Estuary. Marine Geology 343, 1-14.

Fujino, S., Naruse, H., Matsumoto, D., Jarupongsakul, T., Sphawajruksakul, A., Sakakura, N., 2009. Stratigraphic evidence for pre-2004 tsunamis in southwestern Thailand. Marine Geology 262, 25-28.

Fujino, S., Naruse, H., Matsumoto, D., Sakakura, N., Suphawajruksakul, A., Jarupongsakul, T., 2010. Detailed measurements of thickness and grain size of a widespread onshore tsunami deposit in Phang-nga Province, southwestern Thailand. Island Arc 19, 389-398.

Fujino, S., Naruse, H., Suphawajruksakul, A., Jarupongsakul, T., Murayama, M., Ichihara, T., 2008. Thickness and grain-size distribution of Indian Ocean Tsunami Deposits at Khao Lak and Phra Thong Island, south-western Thailand, in: Shiki, T., Tsuji, Y., Yamazaki, T., Minoura, K. (Eds.), Tsunamiites - Features and Implications. Elsevier Inc., Amsterdam, pp. 123-132.

Goff, J., Chagué-Goff, C., Nichol, S., Jaffe, B., Dominey-Howes, D., 2012. Progress in palaeotsunami research. Sedimentary Geology 243-244, 70-88.

Goff, J., Dominey-Howes, D., 2013. 13.13 Tsunami, in: Shroder, J.F. (Ed.), Treatise on Geomorphology. Academic Press, San Diego, pp. 204-218.

Goff, J., McFadgen, B.G., Chagué-Goff, C., 2004. Sedimentary differences between the 2002 Easter storm and the 15th-century Okoropunga tsunami, southeastern North Island, New Zealand. Marine Geology 204, 235-250.

Gouramanis, C., Switzer, A.D., Pham, D.T., Rubin, C., Lee, Y.S., Bristow, C., Jankaew, K., 2014a. Thin-bed ground-penetrating radar analysis of preserved modern and palaeotsunami deposits from Phra Thong Island, Thailand, in: Pajewski, L., Craeye, C., Giannopoulos, A., Andre, F., Lambot, S., Slob, E. (Eds.),

15th International Conference on Ground Penetrating Radar, GPR 2014. Institute of Electrical and Electronics Engineers Inc., pp. 1017-1022.

Gouramanis, C., Switzer, A.D., Polivka, P.M., Bristow, C.S., Jankaew, K., Dat, P.T., Pile, J., Rubin, C.M., Yingsin, L., Ildefonso, S.R., Jol, H.M., 2015. Ground penetrating radar examination of thin tsunami beds — A case study from Phra Thong Island, Thailand. Sedimentary Geology 329, 149-165.

Gouramanis, C., Switzer, A.D., Seshachalam, S., Karthikeyan, A., Pham, D.T., Carson, S., Pilarczyk, J., Hussain, S.M., Yap, W., 2014b. Same Same, But Different: Sedimentological Comparison of Recent Storm and Tsunami Deposits from the South-Eastern Coastline of India. Abstract NH21A-3811 presented at 2014 Fall Meeting, AGU, San Francisco, Calif., 15-19 Dec.

Jackson, D.A., 1993. Stopping rules in principal components analysis: a comparison of heuristical and statistical approaches. Ecology 74, 2204-2214.

Jagodziński, R., Sternal, B., Szczuciński, W., Chagué-Goff, C., Sugawara, D., 2012. Heavy minerals in the 2011 Tohoku-oki tsunami deposits-insights into sediment sources and hydrodynamics. Sedimentary Geology 282, 57-64.

Jagodziński, R., Sternal, B., Szczuciński, W., Lorenc, S., 2009. Heavy minerals in the 2004 tsunami deposits on Kho Khao Island, Thailand. Polish Journal of Environmental Studies 18 (1), 103-110.

Jankaew, K., Atwater, B.F., Sawai, Y., Choowong, M., Charoentitirat, T., Martin, M.E., Prendergast, A., 2008. Medieval forewarning of the 2004 Indian Ocean tsunami in Thailand. Nature 455, 1228-1231.

Jankaew, K., Brill, D., Martin, M.E., Sawai, Y., 2011. Distribution and sedimentary characteristics of tsunami depostits on Phra Thong Island, Thailand, 2nd INQUA-IGCP-567 International Workshop on Active Tectonics, Earthquake Geology, Archaeology and Engineering, Corinth, Greece, pp. 99-101.

Kaufman, L., Rousseeuw, P.J., 2005. Finding groups in data : an introduction to cluster analysis. Wiley, Hoboken, N.J.

Kortekaas, S., Dawson, A.G., 2007. Distinguishing tsunami and storm deposits: an example from Martinhal, SW Portugal. Sedimentary Geology 200, 208-221.

Kuwatani, T., Nagata, K., Okada, M., Watanabe, T., Ogawa, Y., Komai, T., Tsuchiya, N., 2014. Machine-learning techniques for geochemical discrimination of 2011 Tohoku tsunami deposits. Scientific Reports 4.

Legendre, P., Legendre, L., 2012. Numerical ecology. Amsterdam : Elsevier, 2012.

Third English edition.

Liu, K., Fearn, M.L., 2000. Reconstruction of prehistoric landfall frequencies of catastrophic hurricanes in northwestern Florida from lake sediment records. Quaternary Research 54, 238-245.

Maechler, M., Rousseeuw, P., Struyf, A., Hubert, M., Hornik, K., 2014. Cluster: Cluster Analysis Basics and Extensions. R package version 1.15.3. https://cran.r-project.org/web/packages/cluster/index.html

Minoura, K., Imamura, F., Sugawara, D., Kono, Y., Iwashita, T., 2001. The 869 Jogan tsunami deposit and recurrence interval of large-scale tsunami on the Pacific coast of northeast Japan. Journal of Natural Disaster Science 23, 83-88.

Monecke, K., Finger, W., Klarer, D., Kongko, W., McAdoo, B.G., Moore, A.L., Sudrajat, S.U., 2008. A 1,000-year sediment record of tsunami recurrence in northern Sumatra. Nature 455, 1232-1234.

Morton, R.A., Gelfenbaum, G., Jaffe, B.E., 2007. Physical criteria for distinguishing sandy tsunami and storm deposits using modern examples. Sedimentary Geology 200, 184-207.

Nanayama, F., Shigeno, K., Satake, K., Shimokawa, K., Koitabashi, S., Miyasaka, S., Ishii, M., 2000. Sedimentary differences between the 1993 Hokkaido-nansei-oki tsunami and the 1959 Miyakojima typhoon at Taisei, southwestern Hokkaido, northern Japan. Sedimentary Geology 135, 255-264.

Nott, J., 2011. A 6000 year tropical cyclone record from Western Australia. Quaternary Science Reviews 30, 713-722.

Oksanen, J., Blanchet, F.G., Kindt, R., Legendre, P., Minchin, P.R., O'Hara, R.B., Simpson, G.L., Solymos, P., Wagner, M.H.H.S.H., 2016. Vegan: Community Ecology Package. https://CRAN.R-project.org/package=vegan

Phantuwongraj, S., Choowong, M., 2012. Tsunamis versus storm deposits from Thailand. Natural Hazards 63, 31-50.

Prendergast, A., Cupper, M., Jankaew, K., Sawai, Y., 2012. Indian Ocean tsunami recurrence from optical dating of tsunami sand sheets in Thailand. Marine Geology 295-298, 20-27.

R Core Team, 2014. R: A language and environment for statistical computing. http://www.R-project.org/ .

Rousseeuw, P.J., 1987. Silhouettes: a graphical aid to the interpretation and validation of cluster analysis. Journal of Computational and Applied Mathematics 20, 53-65.

Sawai, Y., Jankaew, K., Martin, M.E., Prendergast, A., Choowong, M., Charoentitirat, T., 2009. Diatom assemblages in tsunami deposits associated with the 2004 Indian Ocean tsunami at Phra Thong Island, Thailand. Marine Micropaleontology 73, 70-79.

Scheffers, A., Brill, D., Kelletat, D., Brückner, H., Scheffers, S., Fox, K., 2012. Holocene sea levels along the Andaman Sea coast of Thailand. Holocene 22, 1169-1180.

Shanmugam, G., 2012. Process-sedimentological challenges in distinguishing paleo-tsunami deposits. Natural Hazards 63, 5-30.

Spiske, M., Piepenbreier, J., Benavente, C., Bahlburg, H., 2013. Preservation potential of tsunami deposits on arid siliciclastic coasts. Earth-Science Reviews 126, 58-73.

Sugawara, D., Goto, K., Jaffe, B.E., 2014. Numerical models of tsunami sediment transport — current understanding and future directions. Marine Geology 352, 295-320.

Switzer, A.D., Jones, B.G., 2008. Large-scale washover sedimentation in a freshwater lagoon from the southeast Australian coast: sea-level change, tsunami or exceptionally large storm? Holocene 18, 787-803.

Switzer, A.D., Pucillo, K., Haredy, R.A., Jones, B.G., Bryant, E.A., 2005. Sea level, storm, or tsunami: Enigmatic sand sheet deposits in a sheltered coastal embayment from Southeastern New South Wales, Australia. Journal of Coastal Research 21, 655-663.

Switzer, A.D., Srinivasalu, S., Thangadurai, N., Ram Mohan, V., 2012. Bedding structures in Indian tsunami deposits that provide clues to the dynamics of tsunami inundation. Geological Society Special Publication 361, 61-77.

Switzer, A.D., Yu, F., Gouramanis, C., Soria, J., Pham, T.D., 2014. An integrated approach to assessing coastal hazards at multi-century timescales. Journal of Coastal Research Special Issue No.70, 723-728.

Syvitski, J.P.M., Kettner, A.J., Overeem, I., Hutton, E.W.H., Hannon, M.T., Brakenridge, G.R., Day, J., Vorosmarty, C., Saito, Y., Giosan, L., Nicholls, R.J., 2009. Sinking deltas due to human activities. Nature Geoscience 2, 681-686.

Szczuciński, W., Chaimanee, N., Niedzielski, P., Rachlewicz, G., Saisuttichai, D., Tepsuwan, T., Lorenc, S., Siepak, J., 2006. Environmental and geological impacts of the 26 December 2004 tsunami in coastal zone of Thailand - overview of short and long-term effects. Polish Journal of Environmental Studies 15, 793-810.

Szczuciński, W., Niedzielski, P., Kozak, L., Frankowski, M., Zioła, A., Lorenc, S., 2007. Effects of rainy season on mobilization of contaminants from tsunami deposits left in a coastal zone of Thailand by the 26 December 2004 tsunami. Environmental Geology 53, 253-264.

Szczuciński, W., Niedzielski, P., Rachlewicz, G., Sobczyński, T., Zioła, A., Kowalski, A., Lorenc, S., Siepak, J., 2005. Contamination of tsunami sediments in a coastal zone inundated by the 26 December 2004 tsunami in Thailand. Environmental Geology 49, 321-331.

Tabachnick, B.G., Fidell, L.S., 2013. Using multivariate statistics, sixth ed. Pearson Education, Boston.

Tanaka, G., Naruse, H., Yamashita, S., Arai, K., 2012. Ostracodes reveal the sea-bed origin of tsunami deposits. Geophysical Research Letters 39, doi:10.1029/2012GL051320.

Thai Meteorological Department, 2007. Report for 40th Session of ESCAP/WMO Typhoon Committee, 40th Session of Typhoon Committee, 21-26 November, Macao http://severe.worldweather.org/tcc/creport.htm.

Thai Meteorological Department, 2012. Climate of Thailand, Bangkok http://www.tmd.go.th/en/archive/thailand_climate.pdf.

Tsuji, Y., Namegaya, Y., Matsumoto, H., Iwasaki, S.-I., Kanbua, W., Sriwichai, M., Meesuk, V., 2006. The 2004 Indian tsunami in Thailand: Surveyed runup heights and tide gauge records. Earth, Planets and Space 58, 223-232.

Tuttle, M.P., Ruffman, A., Anderson, T., Jeter, H., 2004. Distinguishing tsunami from storm deposits in eastern North America: the 1929 Grand Banks tsunami versus the 1991 Halloween storm. Seismological Research Letters 75, 117-131.

Williams, M.L., Jones, B.G., Carr, P.F., 2012. Geochemical consequences of the Permian–Triassic mass extinction in a non-marine succession, Sydney Basin, Australia. Chemical Geology 326–327, 174-188.

Figure captions:

Figure 1: a) The regional map shows the location of Phra Thong Island (Ko Phra Thong - KPT), Thailand (red square); b) the detailed map shows the locations of the

offshore samples, onshore samples and the local bathymetry; c) A close-up view of the pre-2004 onshore samples (yellow dots), storm samples (red triangle), Sand C (green square, samples were collected from 40-43 cm depth from a pit), Sand D (orange square, samples were collected from 75-77 cm depth from an auger core (A10)) and the Jankaew et al. (2008)'s trench where Sand A and Sand B were taken; d) The stacked tsunami sand sheets from Jankaew et al. (2008)

Figure 2: Surface interpolation maps of the offshore sediment sample grain size parameters (the mean and sorting), quartz mineral (finer fraction) and selected trace elements. Sample labels are shown in Figure 1.

Figure 3: The PAM analysis for grain size parameters. (a) The number of groups and equivalent silhouette width. (b) The clustering structure of sample set, different colours differentiate clusters

Figure 4: The PCA analysis for grain size parameters. (a) The first two principal components (PCA1 versus PCA2); (b) The screeplot shows the ordination analysis (black line) versus the broken stick rule (red line).

Figure 5: The DFA analysis for grain size parameters. The graph shows the first two discriminant function analysis (DF1 versus DF2). The stacked histograms show the scores and power of separation of each group relative to the other groups.

Figure 6: The PAM analysis for mineral contents. (a) The number of groups and equivalent silhouette width. (b) The clustering structure of sample set, different colours differentiate the clusters.

Figure 7: The PCA analysis for mineral contents. (a) The first two principal components PCA1 versus PCA2; (b) PCA1 versus PCA3; (c) PCA2 versus PCA3; (d) The screeplot shows the ordination analysis (black line) versus the broken stick rule (red line).

Figure 8: The DFA analysis for mineral contents. The graph shows the first two discriminant function analysis (DF1 versus DF2). The stacked histograms show the scores and power of separation of each group relative to the other groups.

Figure 9: The PAM analysis for trace elements. (a) The number of groups and equivalent silhouette width. (b) The clustering structure of the sample set, different colours differentiate the clusters.

Figure 10: The PCA analysis for trace elements. (a) The first two principal components PCA1 versus PCA2; (b) PCA1 versus PCA3; (c) PCA2 versus PCA3; (d) The screeplot shows the ordination analysis (black line) versus the broken stick rule (red line).

Figure 11: The DFA analysis for trace elements. The graph shows the first two discriminant function analysis (DF1 versus DF2). The stacked histograms show the scores and power of separation of each group relative to the other groups.

Figure 12: The temporal variations of 22 trace elements between the 2004 IOT and three paleo-tsunami deposits.

Figure S1: Surface interpolation maps of the mineralogy of the offshore sediment samples using the full grain size suite: quartz, aragonite, calcite and garnet.

Figure S2: Surface interpolation maps of the < 0.125mm mineralogy of the offshore sediment samples: aragonite, muscovite, cassiterite, labradorite, kaolin and monazite.

Figure S3: Surface interpolation maps of the < 0.125 mm mineralogy of the offshore sediment samples: zircon, orthoclase and microcline.

Figure S4: Surface interpolation maps of the trace element geochemistry of the offshore sediment samples: U, Th, Rb, La, Nb, Y

Figure S5: Surface interpolation maps of the trace element geochemistry of the offshore sediment samples: As, Cr, Pb, V, Ba and Cu

Figure S6: Surface interpolation maps of the trace element geochemistry of the offshore sediment samples: Bi, Hf, Se, Cs, Ga and Ni.

Figure S7: Bootstrap analysis of PC1 (two top panels) and PC2 (two bottom panels) of the grain size data showing a) a quantile plot and b) a histogram of the bootstrapped eigenvalues (λ*) and showing the bootstrapped confidence interval (red lines), mean of the bootstrapped eigenvalue (λ*black solid line) and determined eigenvalue (λ*green dashed line).

Figure S8: Bootstrap analysis of PC1 (two top panels) and PC2 (two bottom panels) of the mineralogy data showing a) a quantile plot and b) a histogram of the bootstrapped eigenvalues (λ*) and showing the bootstrapped confidence interval (red lines), mean of the bootstrapped eigenvalue (λ*black solid line) and determined eigenvalue (λ*green dashed line).

Figure S9: Bootstrap analysis of PC3 of the mineralogy data showing a) a quantile plot and b) a histogram of the bootstrapped eigenvalues (λ*) and showing the bootstrapped confidence interval (red lines), mean of the bootstrapped eigenvalue (λ*black solid line) and determined eigenvalue (λ*green dashed line).

Figure S10: Bootstrap analysis of PC1 (two top panels) and PC2 (two bottom panels) of the geochemistry data showing a) a quantile plot and b) a histogram of the bootstrapped eigenvalues (λ*) and showing the bootstrapped confidence interval (red lines), mean of the bootstrapped eigenvalue (λ*black solid line) and determined eigenvalue (λ*green dashed line).

Table captions:

Table 1: Grain size parameters (mean, sorting, skewness and kurtosis) of sediment samples performed using the Malvern Mastersizer 2000.

Table 2: Mineral contents of finer fraction (in wt. %).

Table 3: Trace element concentrations of bulk samples (in ppm).

Table S1: Table showing for each principal component of the grain size data the eigenvalues (λ), the percent variance explained by each eigenvalue and whether the Kaiser-Guttman criteria defines the principal component as significant or not (Legendre and Legendre, 2012).

Table S2: Table showing for each principal component of the mineralogy data the eigenvalues (λ), the percent variance explained by each eigenvalue and whether the Kaiser-Guttman criteria defines the principal component as significant or not (Legendre and Legendre, 2012).Table S3: Table showing for each principal component of the geochemistry data the eigenvalues (λ), the percent variance explained by each eigenvalue and whether the Kaiser-Guttman criteria defines the principal component as significant or not (Legendre and Legendre, 2012).

Table S4: Correlation coefficients of 22 trace elements used in statistical analyses.

Table S5: Correlation coefficients of the mean grain size and selected trace elements.

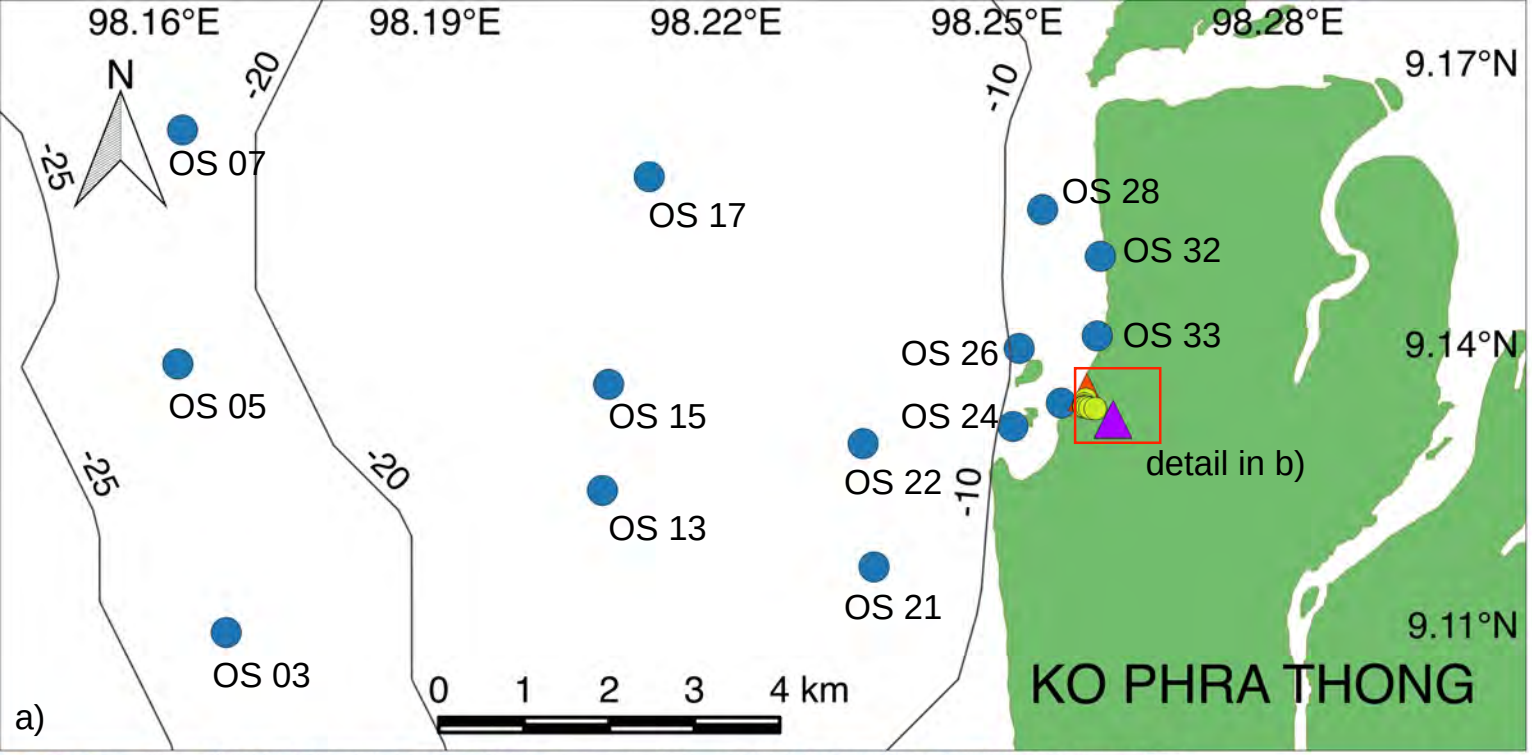

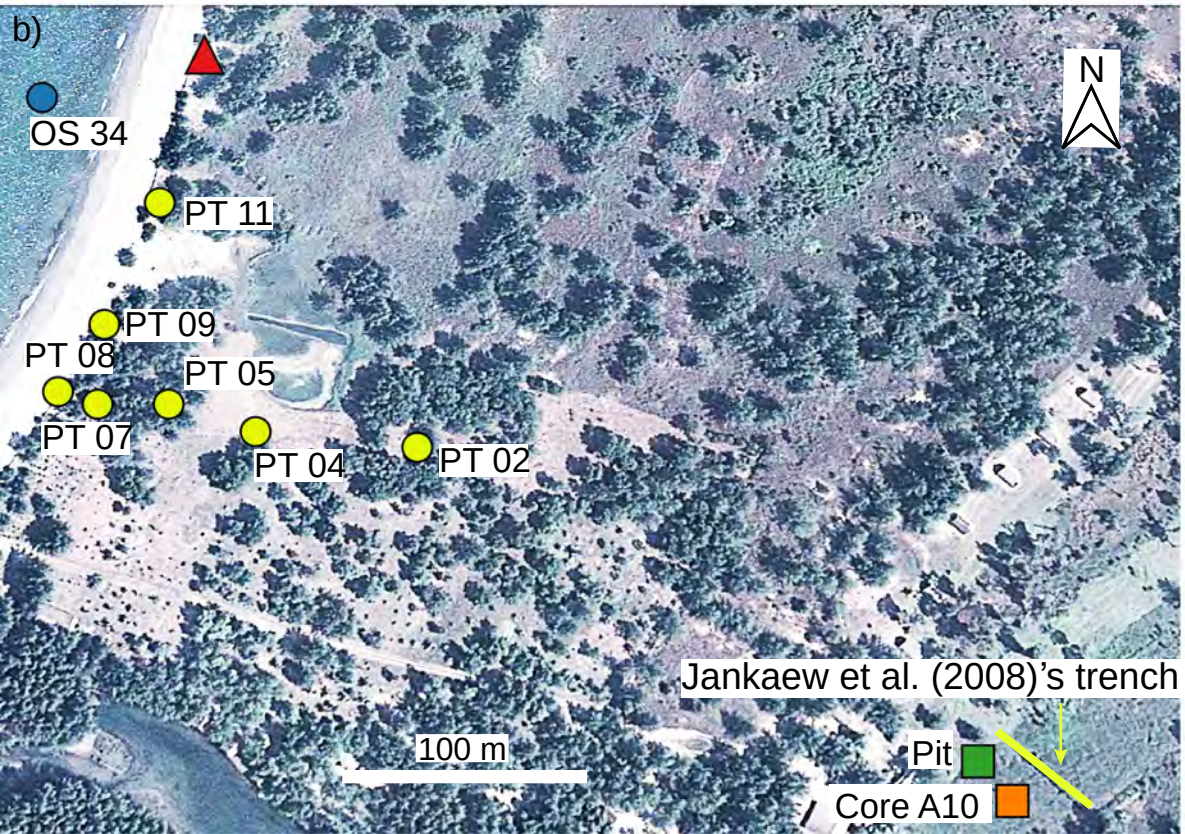

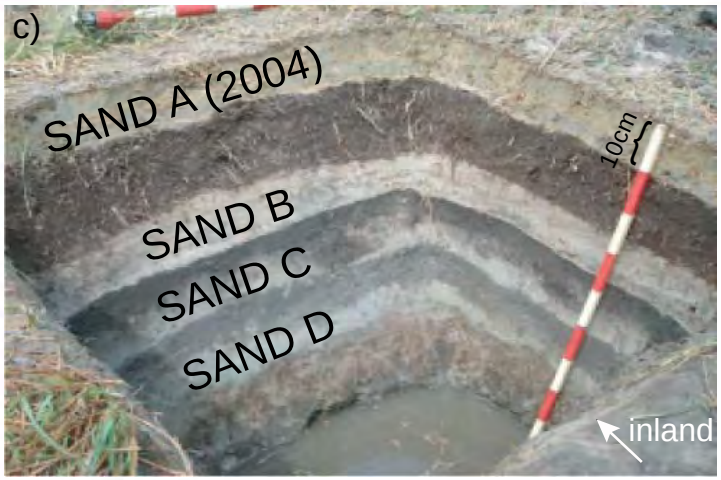

Legend

- Onshore samples
- Storm sample
- Tsunami samples
- Offshore samples
- Water contour depth (m)
- Pit (Sand C samples location)
- Core A10 (Sand D samples location)

Figure 1

a)

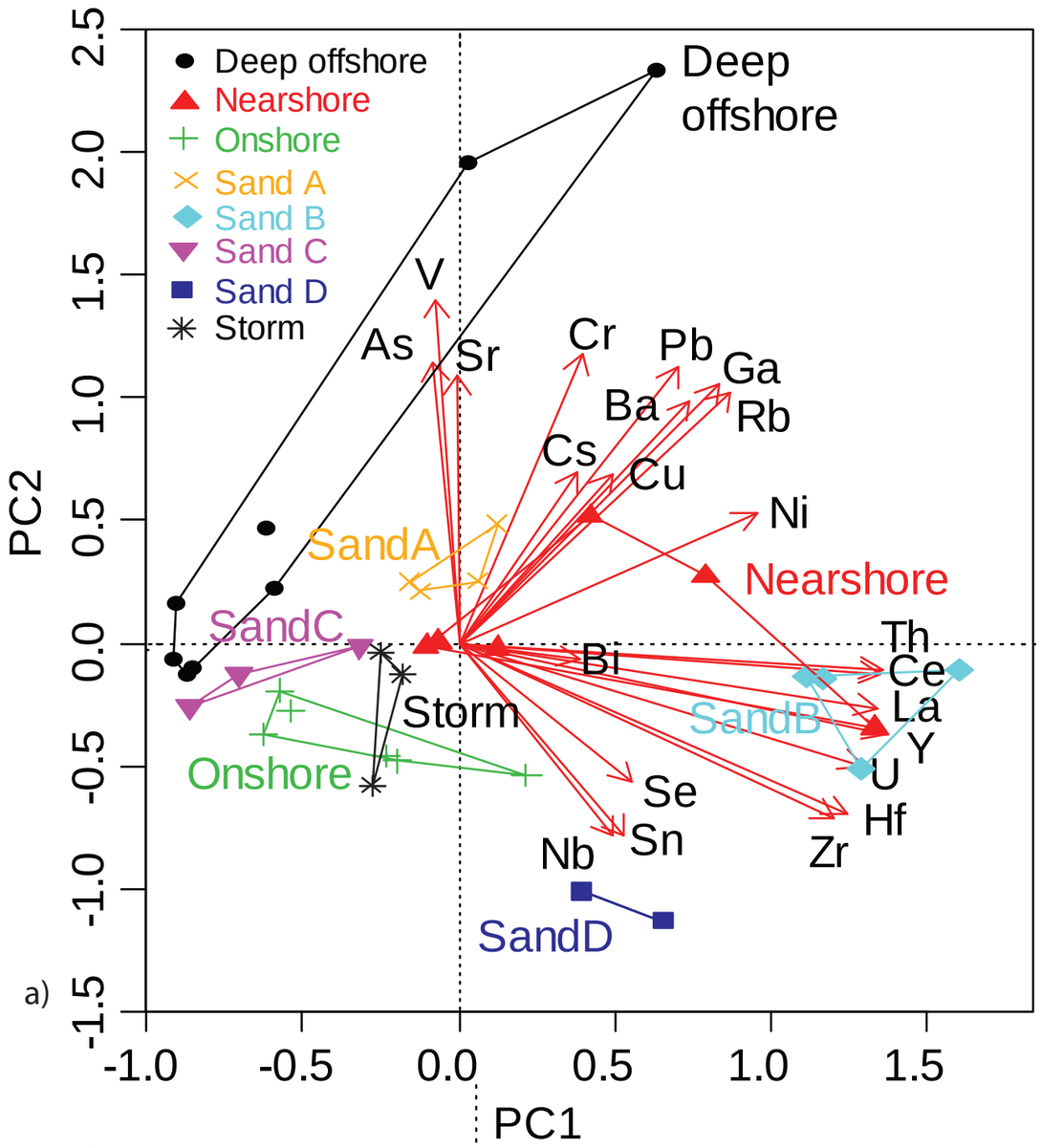
Deep offshore
Nearshore
Onshore
Sand A
Sand B
Sand C
Sand D
Storm
PC2
PC1
Deep offshore
V
As
Sr
Cr
Pb
Ga
Ba
Rb
Cs
Cu
Ni
SandA
Nearshore
SandC
Th
Ce
Bi
La
Storm
SandB
Y
Onshore
U
Se
Hf
Sn
Zr
Nb
SandD

b)

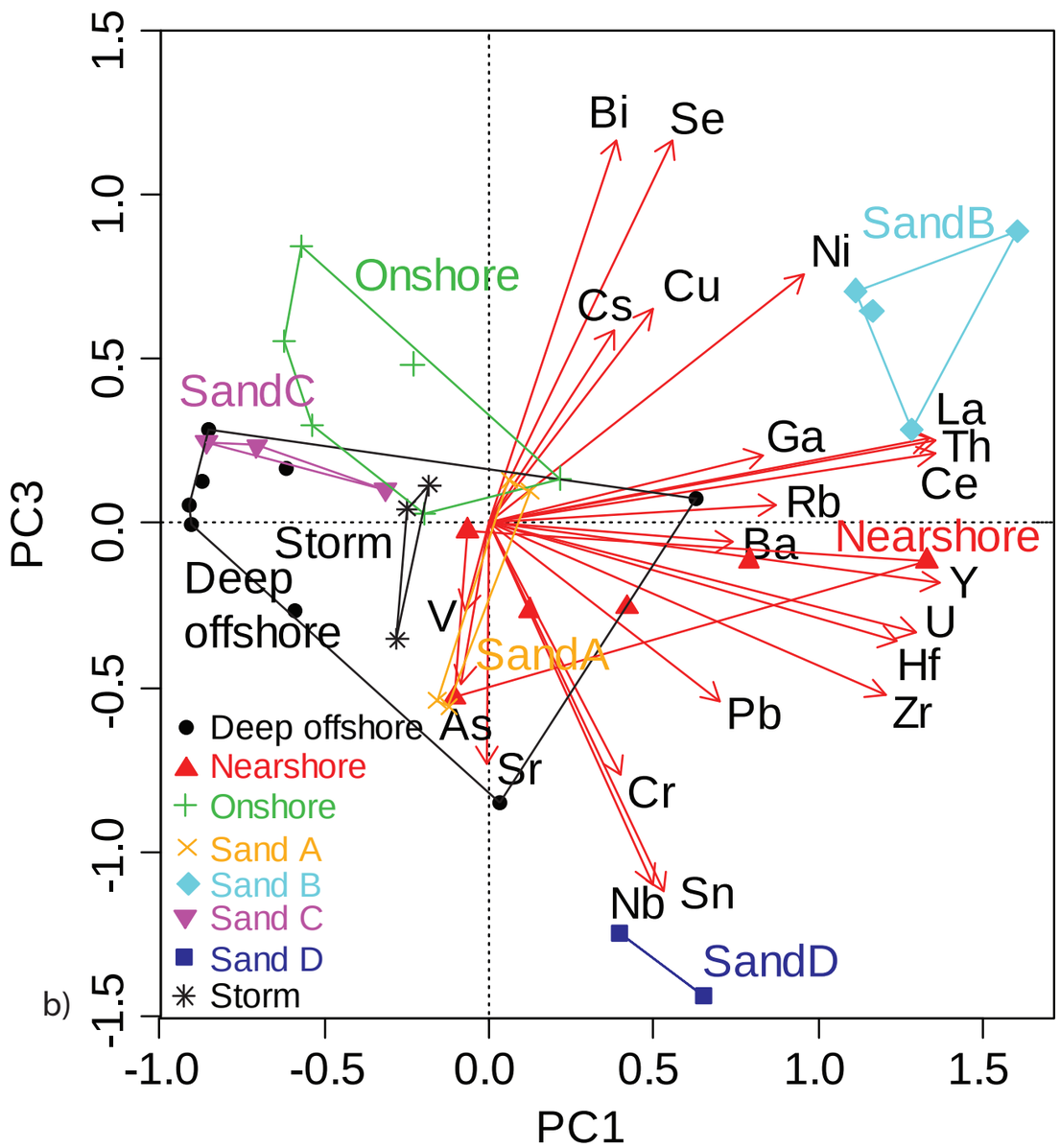
PC3
PC1
Bi
Se
Onshore
Ni
SandB
Cs
Cu
SandC
La
Th
Ce
Ga
Rb
Storm
Ba
Nearshore
Deep offshore
Y
V
U
Hf
SandA
Pb
Zr
As
Deep offshore
Nearshore
Onshore
Sand A
Sand B
Sand C
Sand D
Storm
Sr
Cr
Nb
Sn
SandD

c)

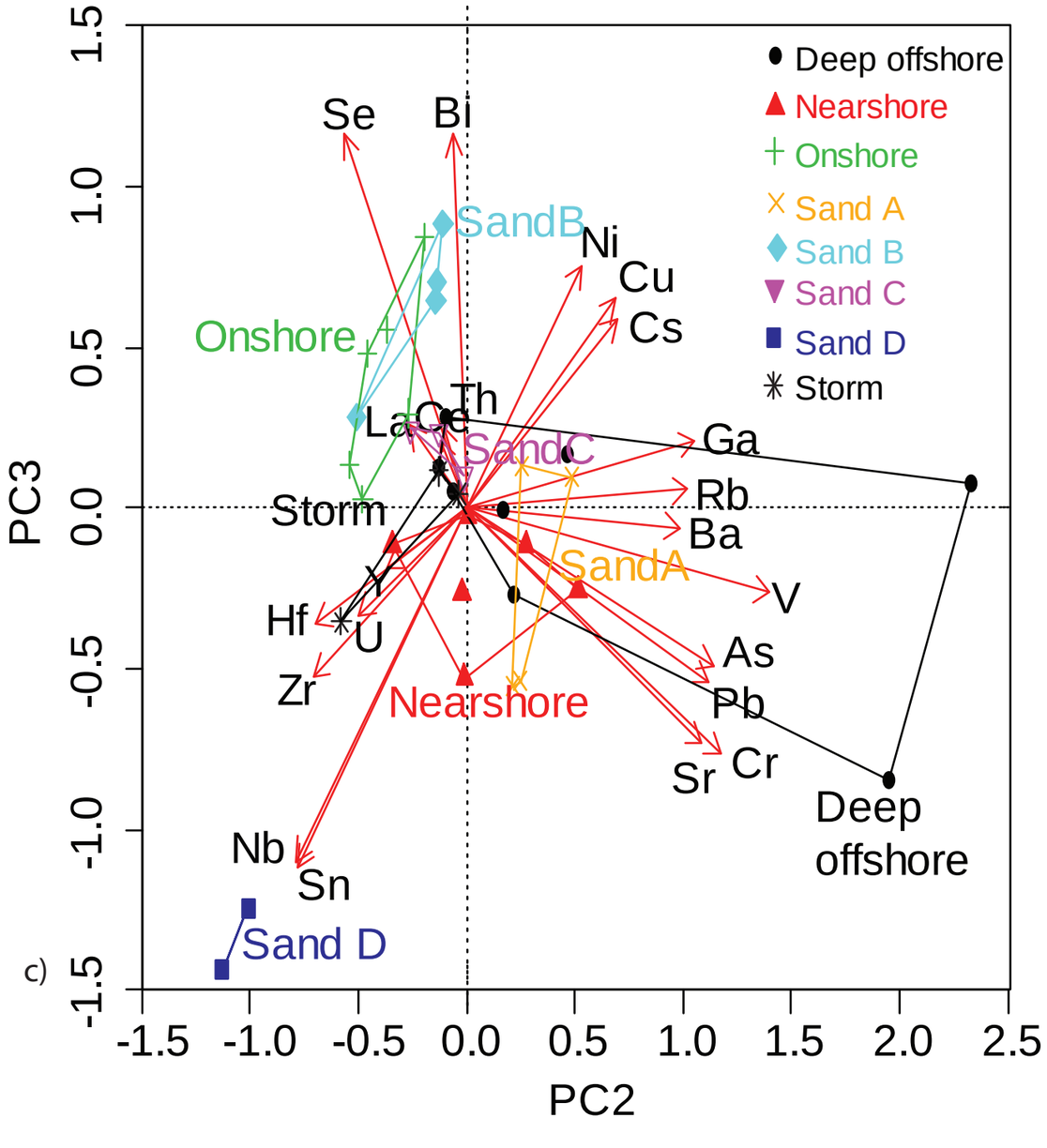
PC3
PC2
Deep offshore
Nearshore
Onshore
Sand A
Sand B
Sand C
Sand D
Storm
Se
Bi
SandB
Ni
Cu
Cs
Onshore
Th
La
Ce
SandC
Ga
Storm
Rb
Ba
SandA
V
Hf
U
As
Zr
Nearshore
Pb
Sr
Cr
Deep offshore
Nb
Sn
Sand D

d)

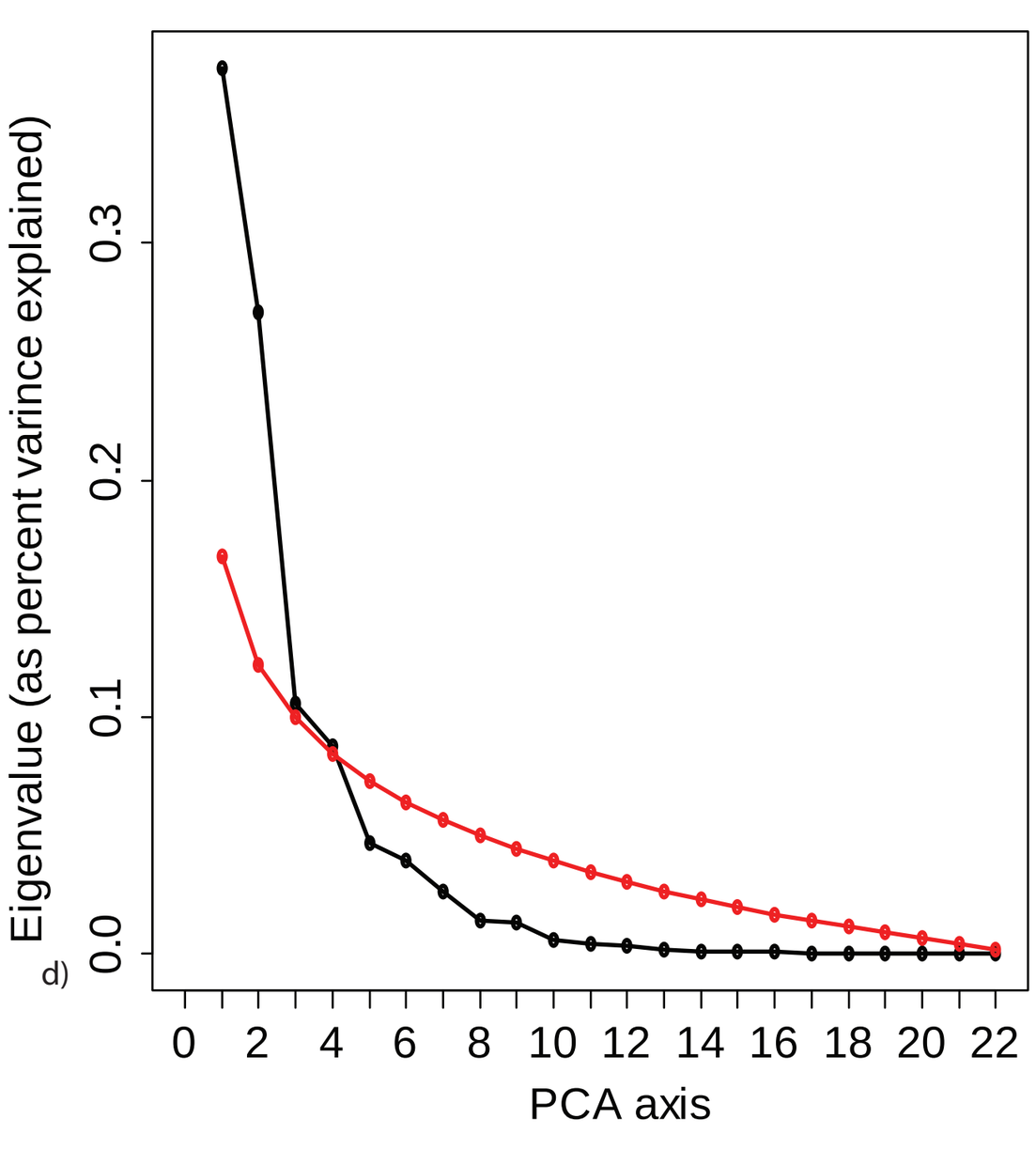
Eigenvalue (as percent varince explained)
PCA axis

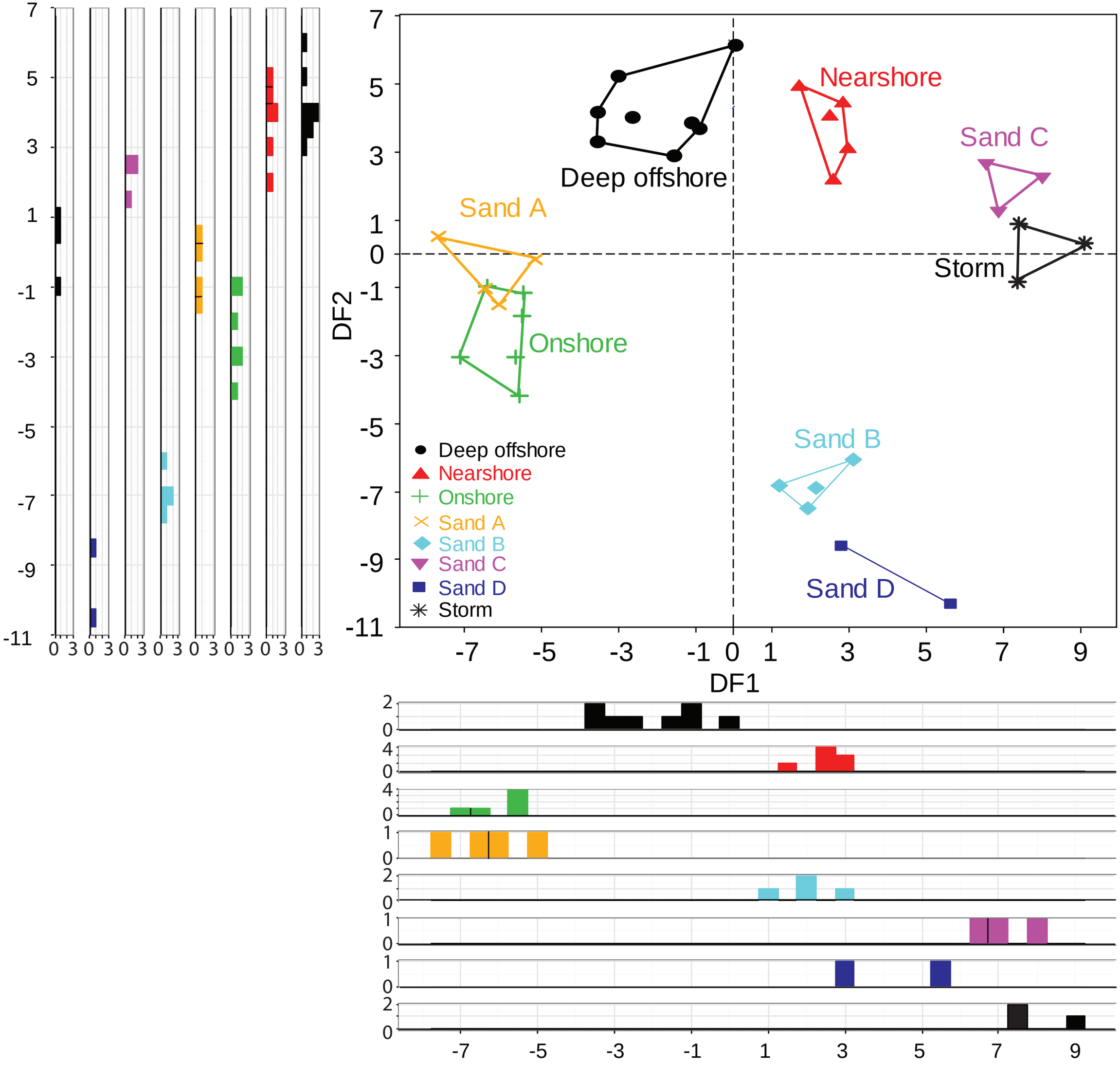
DF2
DF1
Deep offshore
Nearshore
Sand C
Storm
Sand A
Onshore
Sand B
Sand D
Deep offshore
Nearshore
Onshore
Sand A
Sand B
Sand C
Sand D
Storm

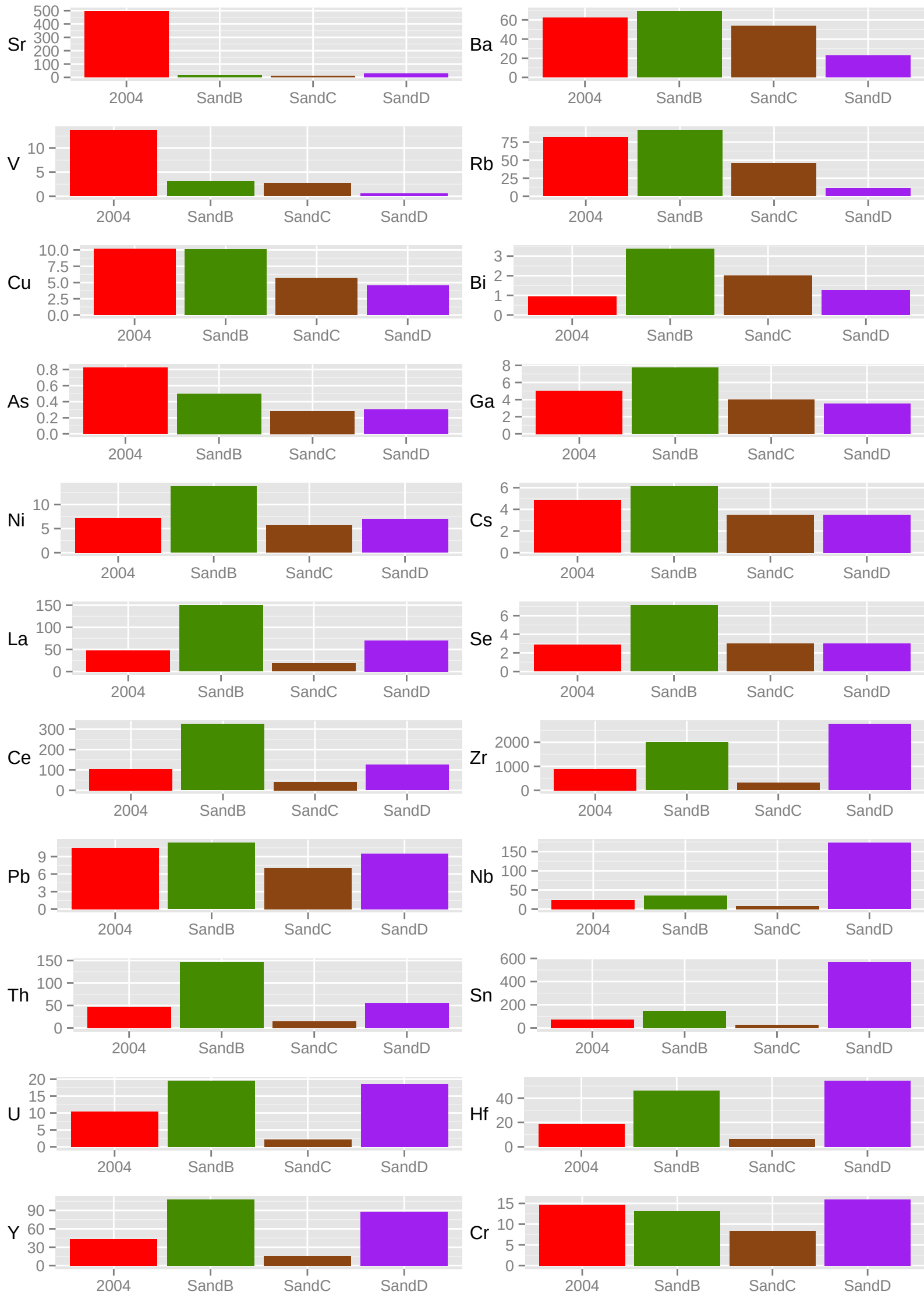
Sr
500
400
300
200
100
0
2004
SandB
SandC
SandD
Ba
60
40
20
0
V
10
5
0
Rb
75
50
25
Cu
10.0
7.5
5.0
2.5
0.0
Bi
3
2
1
As
0.8
0.6
0.4
0.2
Ga
8
6
4
Ni
Cs
La
150
Se
Ce
300
Zr
2000
1000
Pb
9
3
Nb
Th
Sn
600
U
Hf
Y
90
30
Cr
15

Mean grain size (phi)

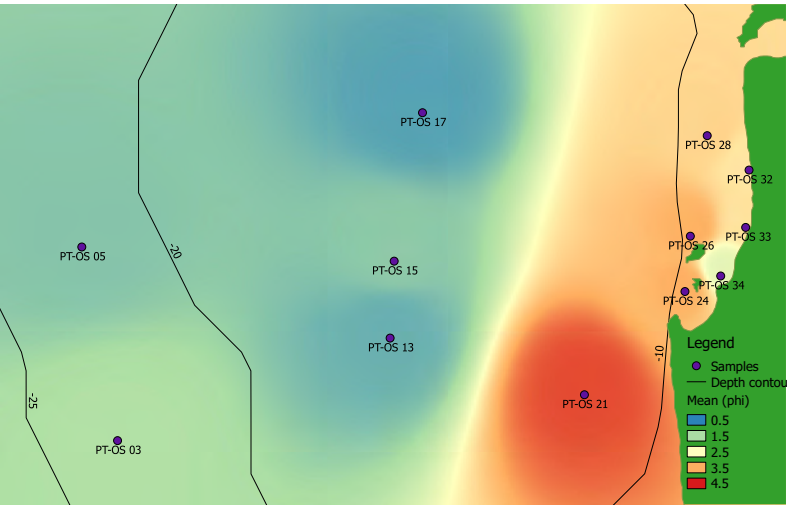

Sorting

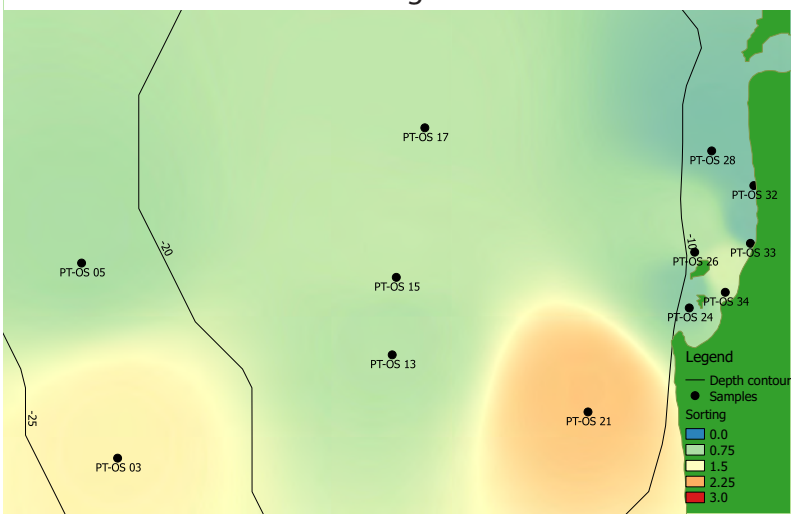

Quartz (wt. %)

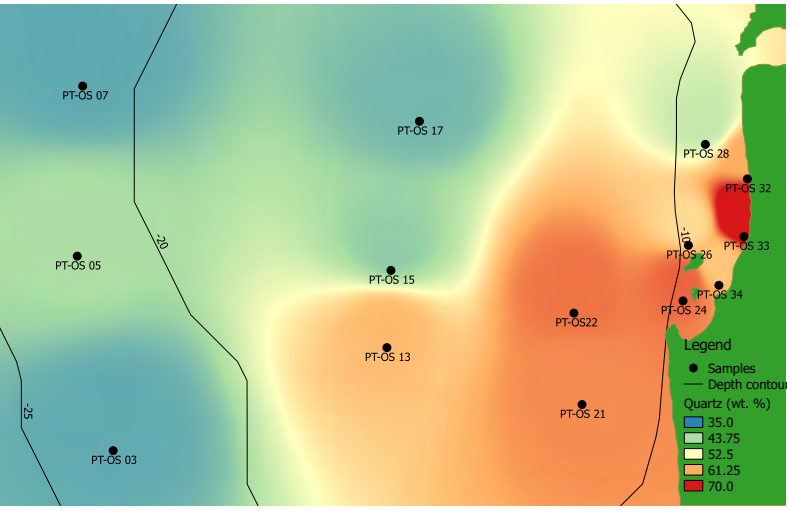

Sr (ppm)

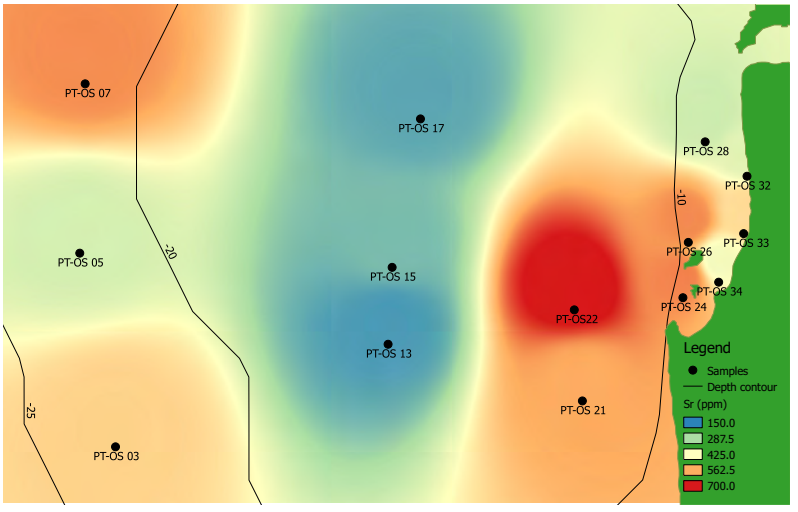

Sn (ppm)

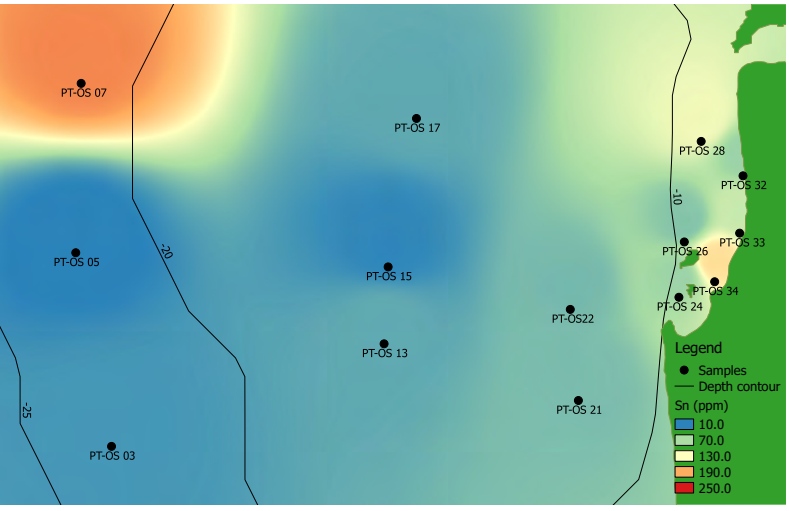

Zr (ppm)

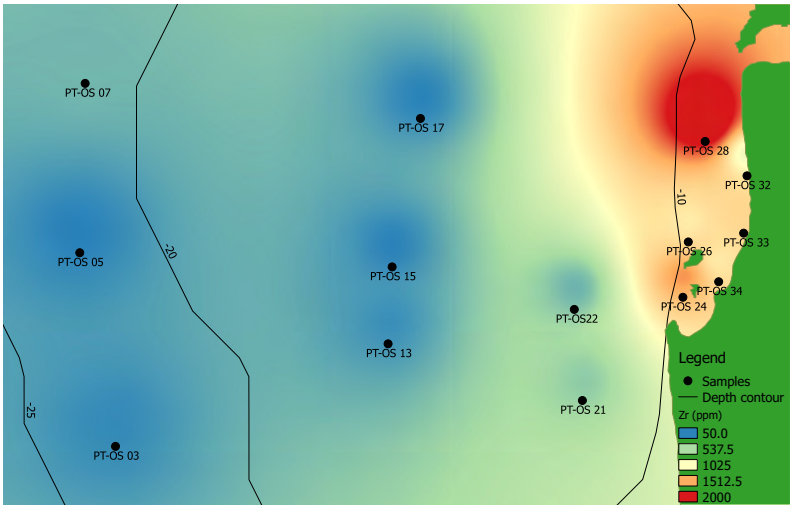

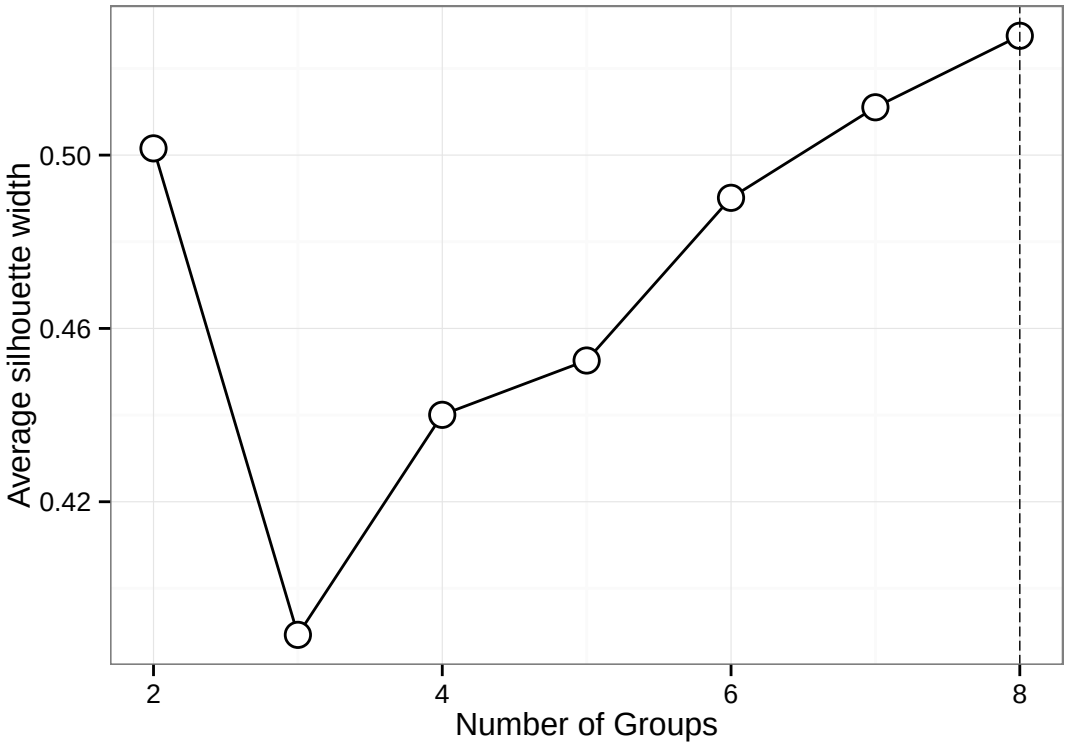
Average silhouette width
0.50
0.46
0.42
2
4
6
8
Number of Groups

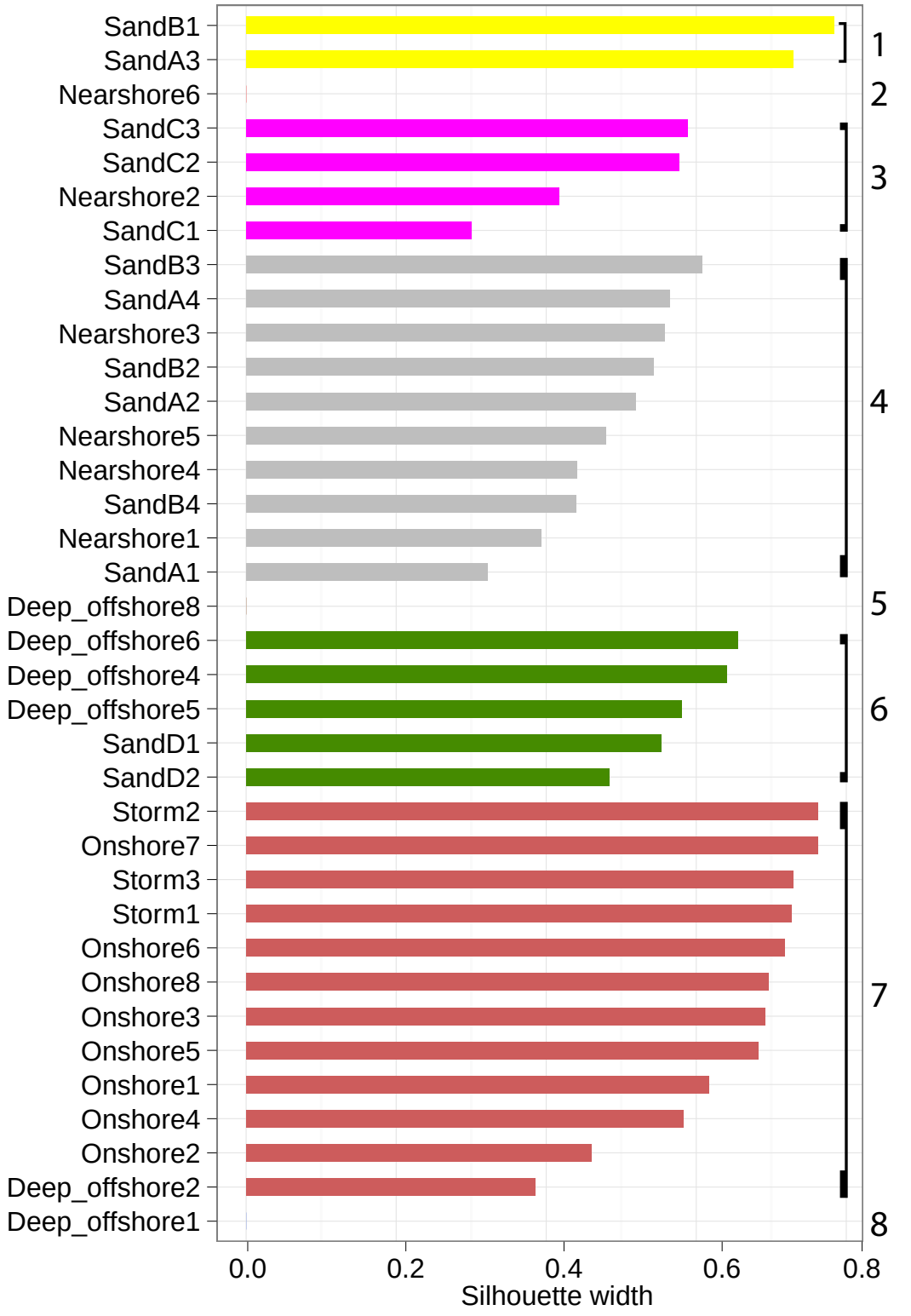
SandB1
SandA3
Nearshore6
SandC3
SandC2
Nearshore2
SandC1
SandB3
SandA4
Nearshore3
SandB2
SandA2
Nearshore5
Nearshore4
SandB4
Nearshore1
SandA1
Deep_offshore8
Deep_offshore6
Deep_offshore4
Deep_offshore5
SandD1
SandD2
Storm2
Onshore7
Storm3
Storm1
Onshore6
Onshore8
Onshore3
Onshore5
Onshore1
Onshore4
Onshore2
Deep_offshore2
Deep_offshore1
1
2
3
4
5
6
7
8
0.0
0.2
0.4
0.6
0.8
Silhouette width

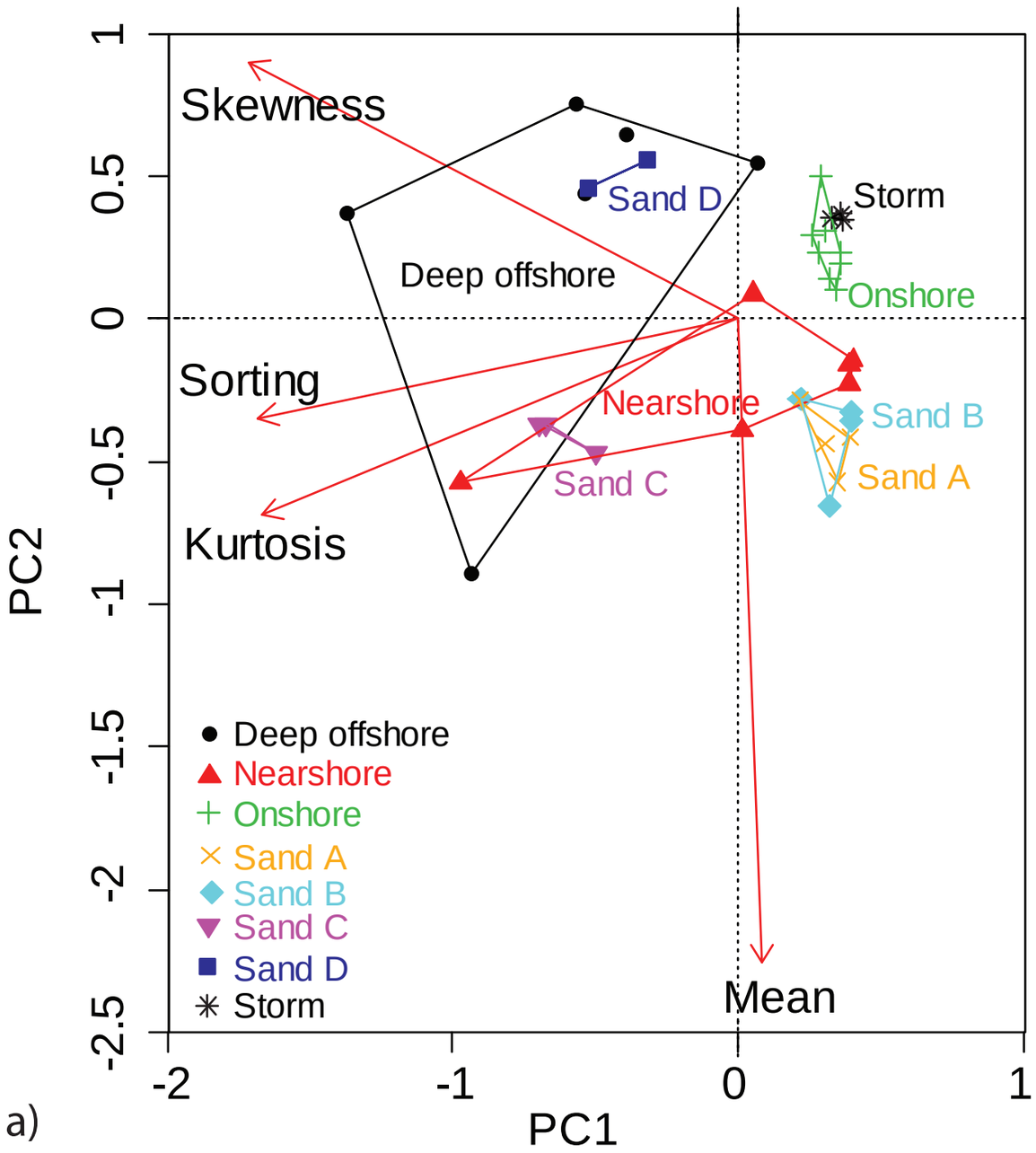
Skewness
Sorting
Kurtosis
Deep offshore
Sand D
Storm
Onshore
Nearshore
Sand B
Sand C
Sand A
Mean
Deep offshore
Nearshore
Onshore
Sand A
Sand B
Sand C
Sand D
Storm
PC2
PC1
1
0.5
0
-0.5
-1
-1.5
-2
-2.5
-2
-1
0
1

a)

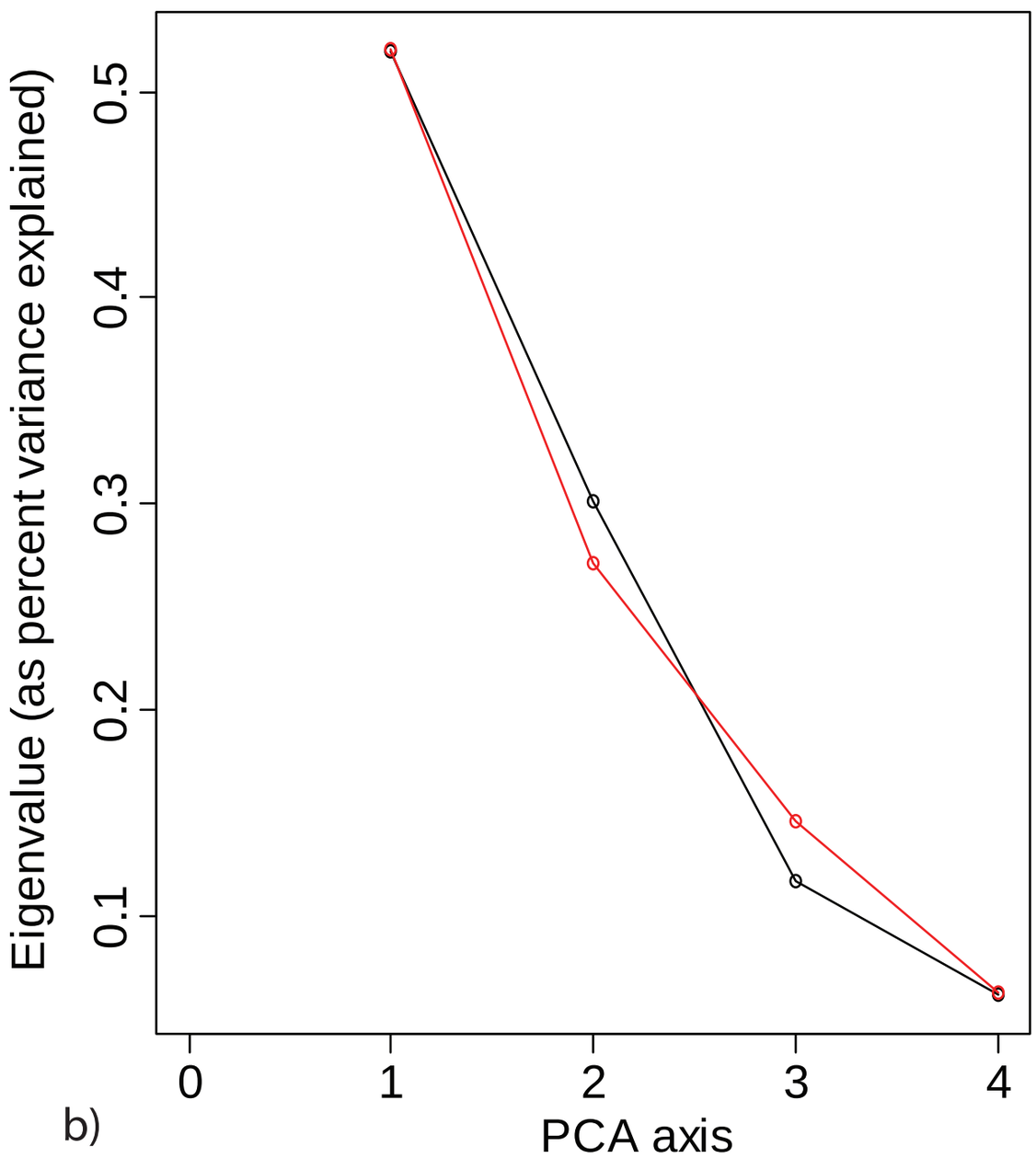
Eigenvalue (as percent variance explained)
PCA axis
0.5
0.4
0.3
0.2
0.1
0
1
2
3
4

b)

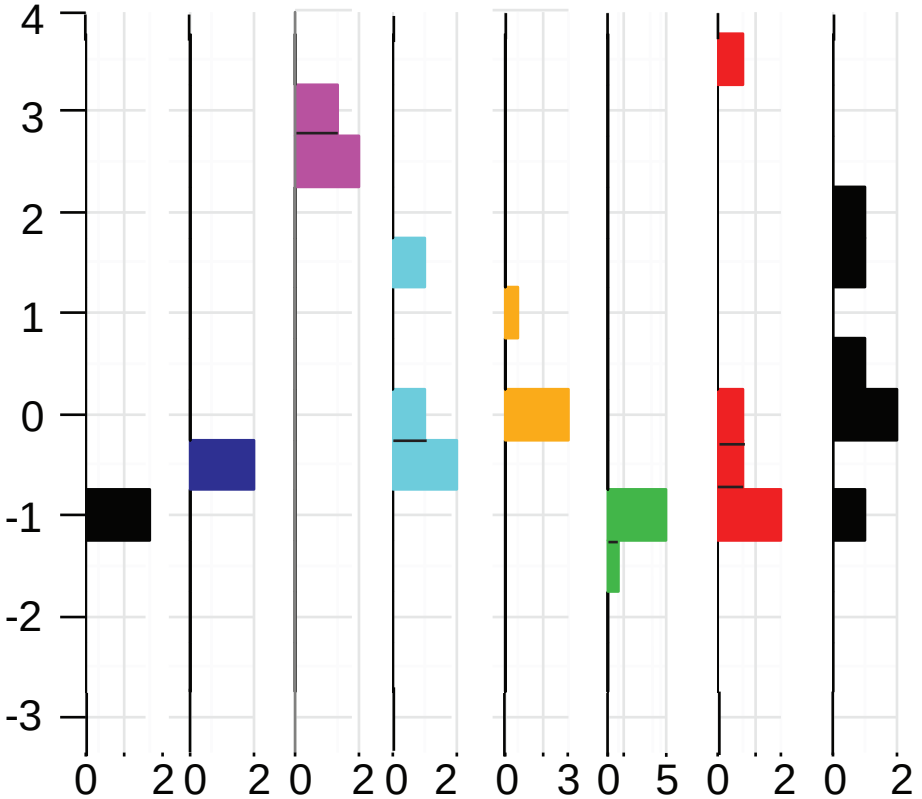

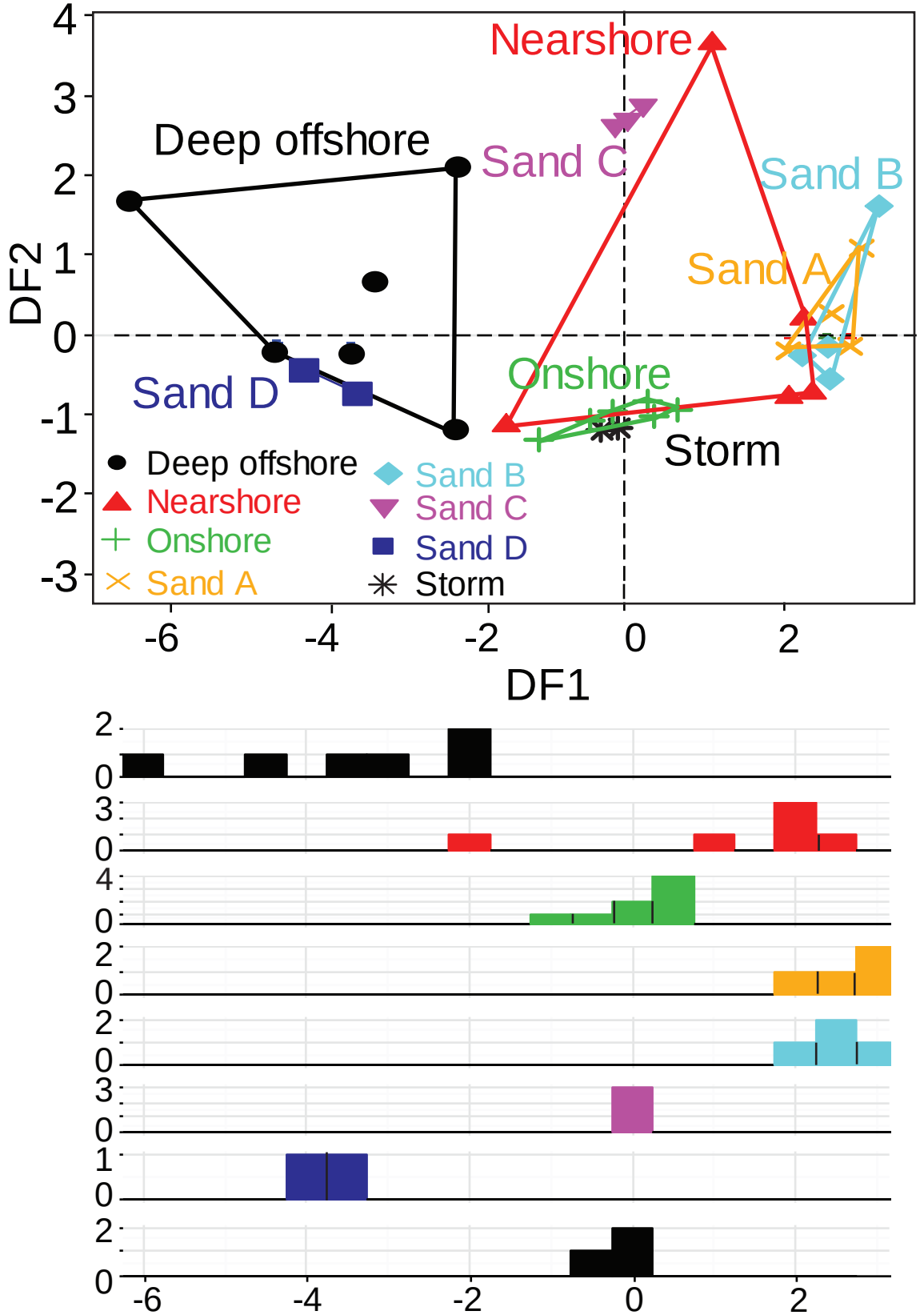
Nearshore
Deep offshore
Sand C
Sand B
Sand A
Onshore
Sand D
Storm
Deep offshore
Nearshore
Onshore
Sand A
Sand B
Sand C
Sand D
Storm
DF1
DF2

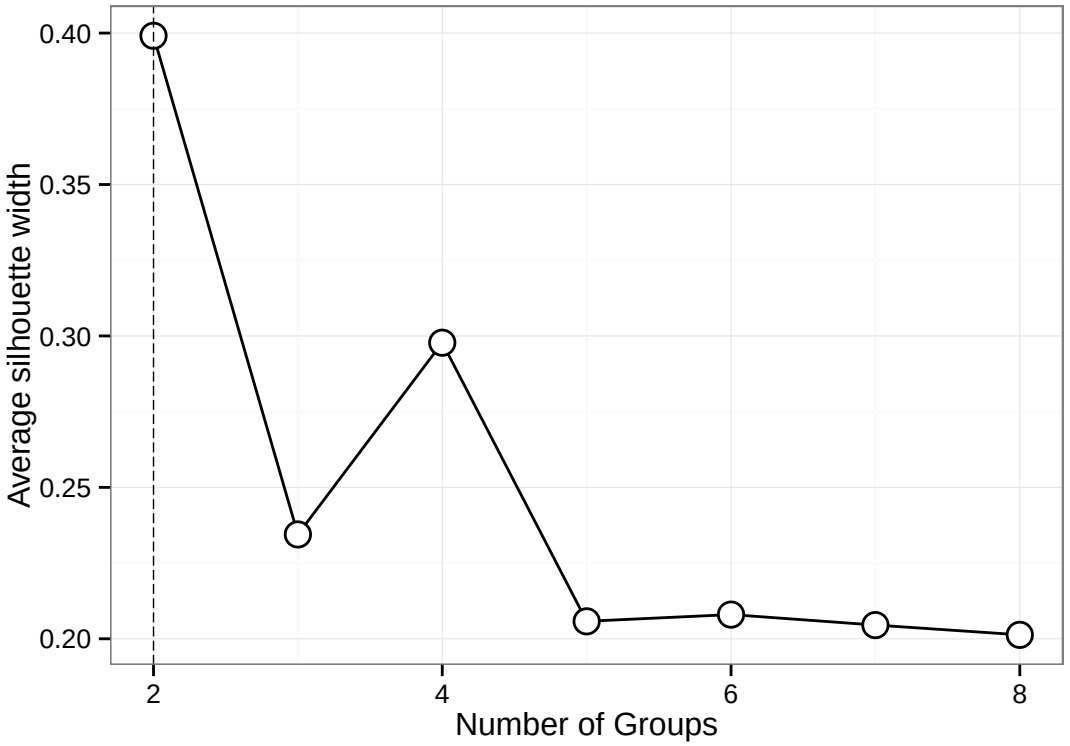
Average silhouette width
0.40
0.35
0.30
0.25
0.20
2
4
6
8
Number of Groups

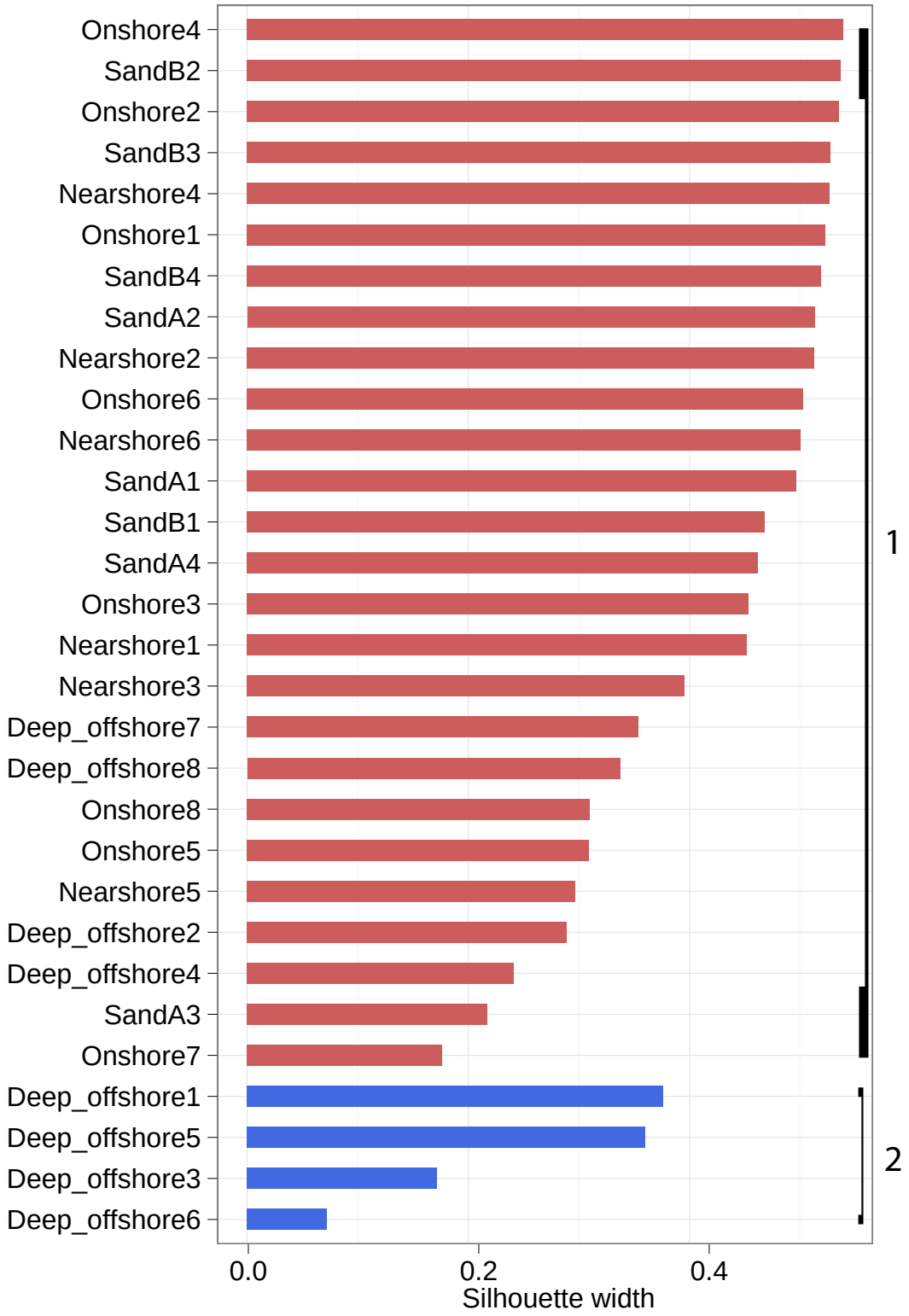
Onshore4
SandB2
Onshore2
SandB3
Nearshore4
Onshore1
SandB4
SandA2
Nearshore2
Onshore6
Nearshore6
SandA1
SandB1
SandA4
Onshore3
Nearshore1
Nearshore3
Deep_offshore7
Deep_offshore8
Onshore8
Onshore5
Nearshore5
Deep_offshore2
Deep_offshore4
SandA3
Onshore7
Deep_offshore1
Deep_offshore5
Deep_offshore3
Deep_offshore6
1
2
0.0
0.2
0.4
Silhouette width

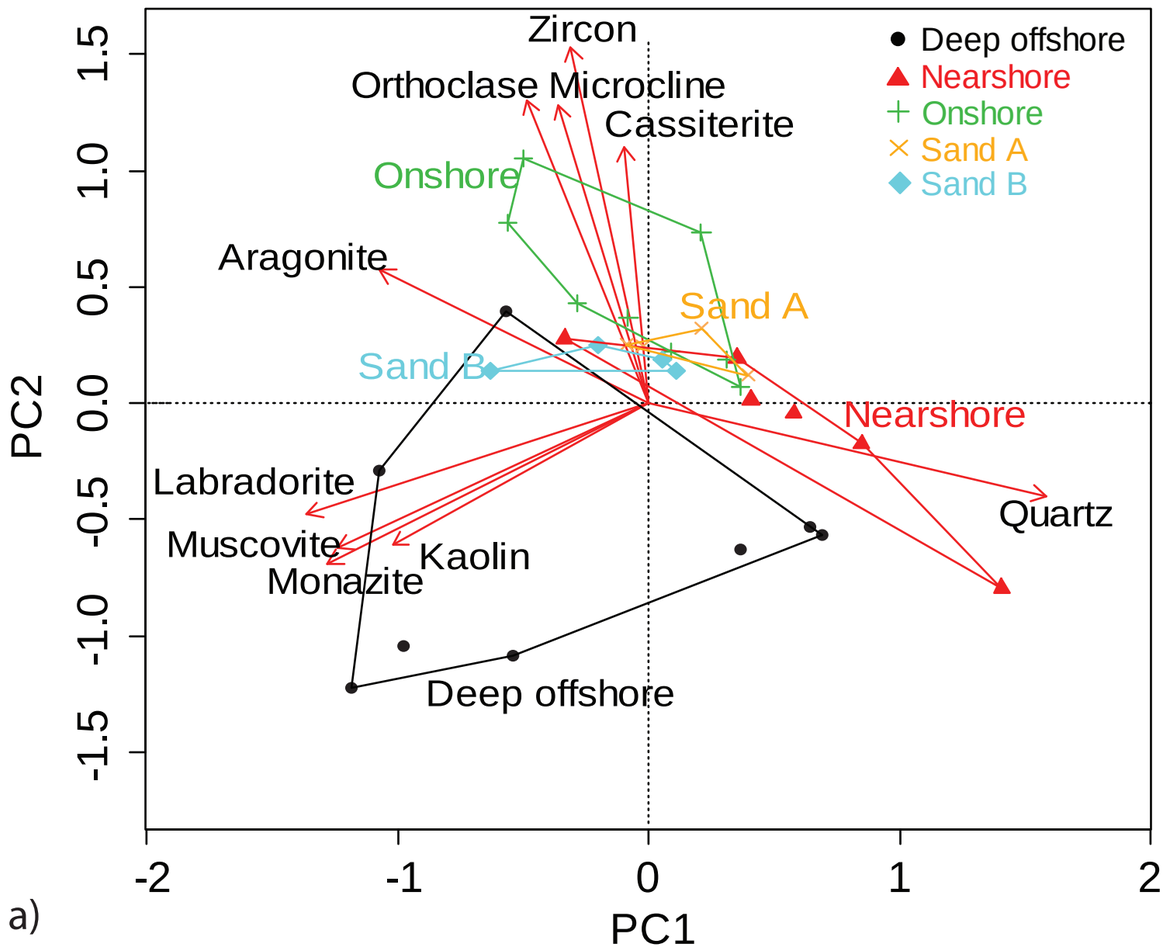
Zircon
Orthoclase Microcline
Cassiterite
Onshore
Aragonite
Sand A
Sand B
Nearshore
Quartz
Labradorite
Muscovite
Kaolin
Monazite
Deep offshore
Deep offshore
Nearshore
Onshore
Sand A
Sand B
PC1
PC2
-2
-1
0
1
2
1.5
1.0
0.5
0.0
-0.5
-1.0
-1.5

a)

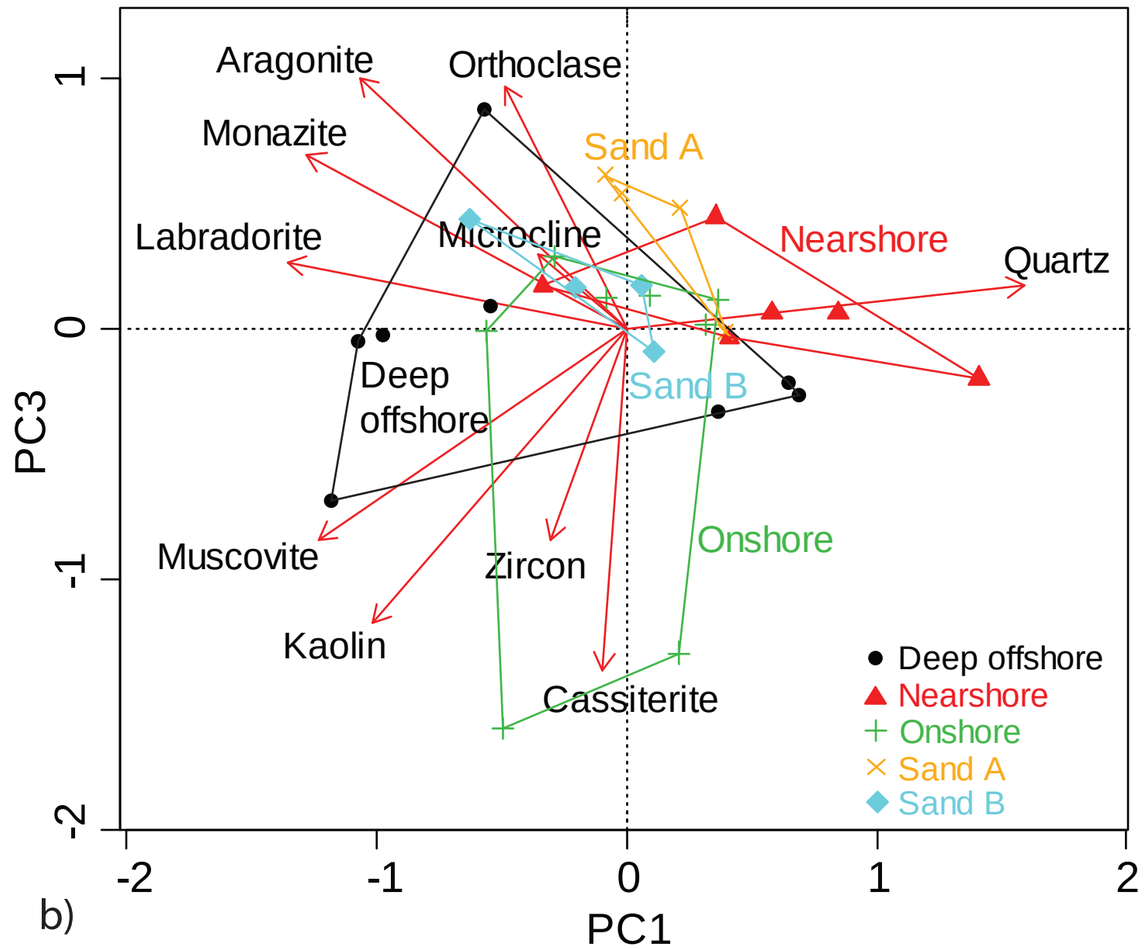
Aragonite
Orthoclase
Monazite
Sand A
Labradorite
Microcline
Nearshore
Quartz
Deep
offshore
Sand B
Muscovite
Zircon
Onshore
Kaolin
Cassiterite
Deep offshore
Nearshore
Onshore
Sand A
Sand B
PC1
PC3
-2
-1
0
1
2

b)

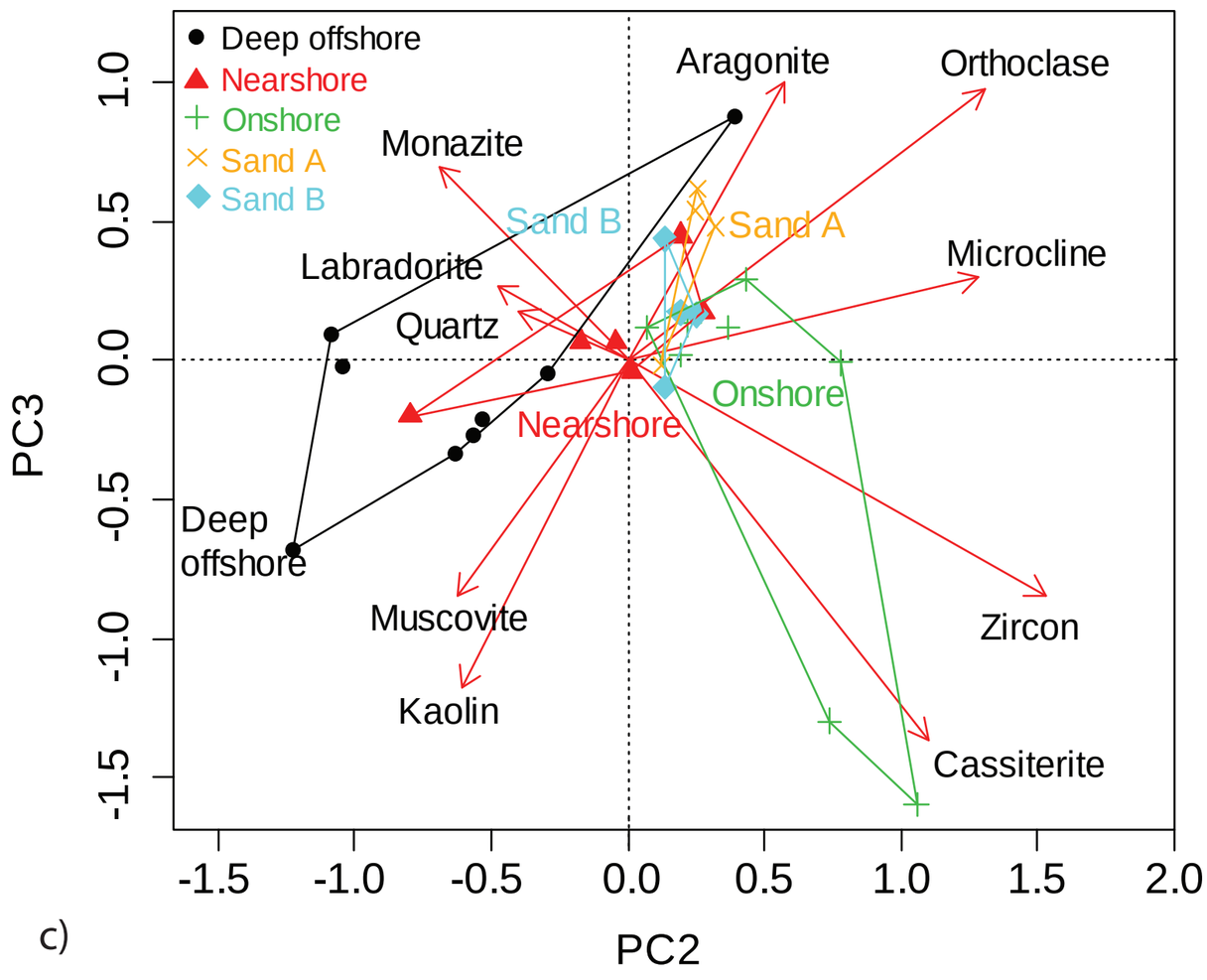
Deep offshore
Nearshore
Onshore
Sand A
Sand B
Aragonite
Orthoclase
Monazite
Sand B
Sand A
Microcline
Labradorite
Quartz
Onshore
Nearshore
Deep
offshore
Zircon
Muscovite
Kaolin
Cassiterite
PC2
PC3
-1.5
-1.0
-0.5
0.0
0.5
1.0
1.5
2.0

c)

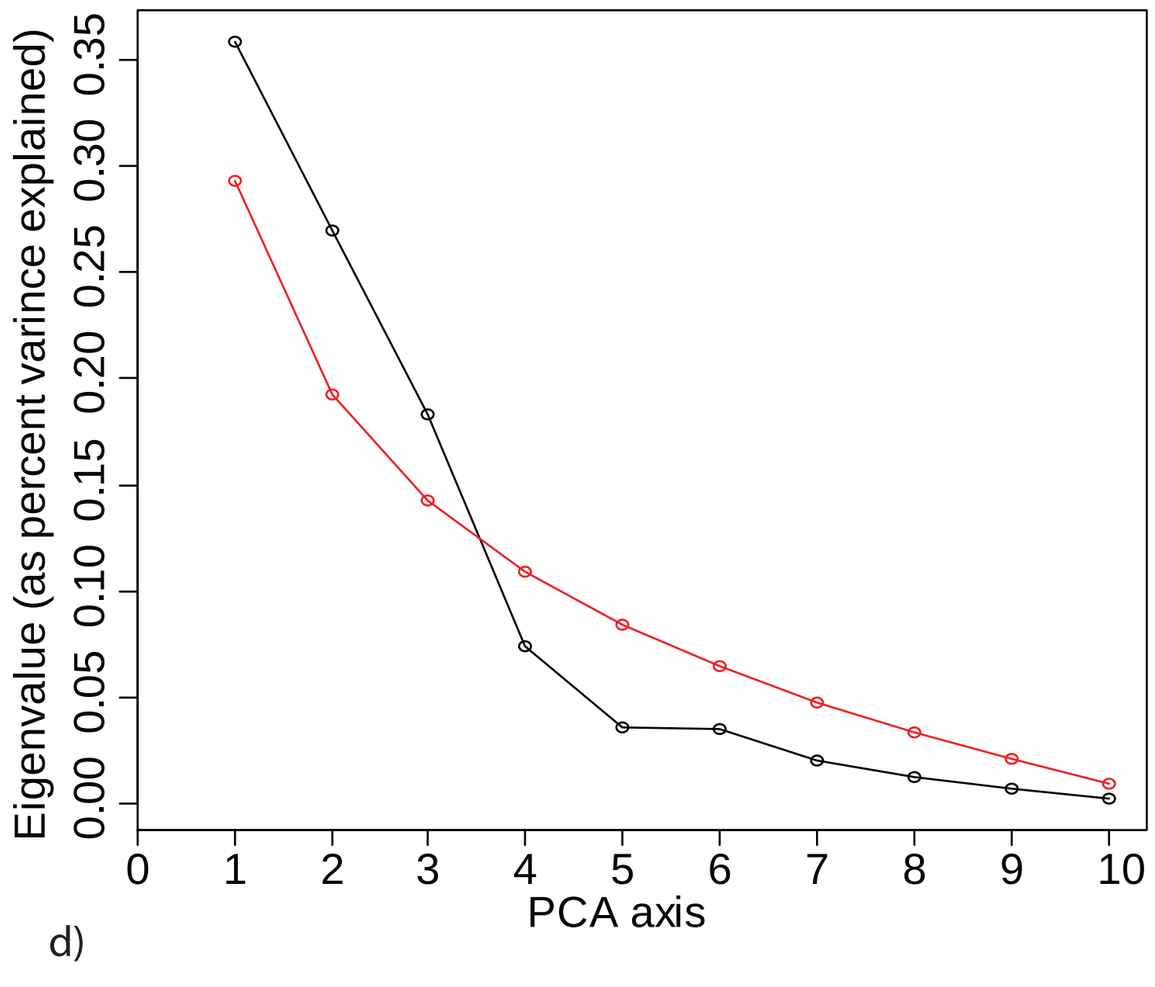
Eigenvalue (as percent varince explained)
PCA axis
0.00
0.05
0.10
0.15
0.20
0.25
0.30
0.35
0
1
2
3
4
5
6
7
8
9
10

d)

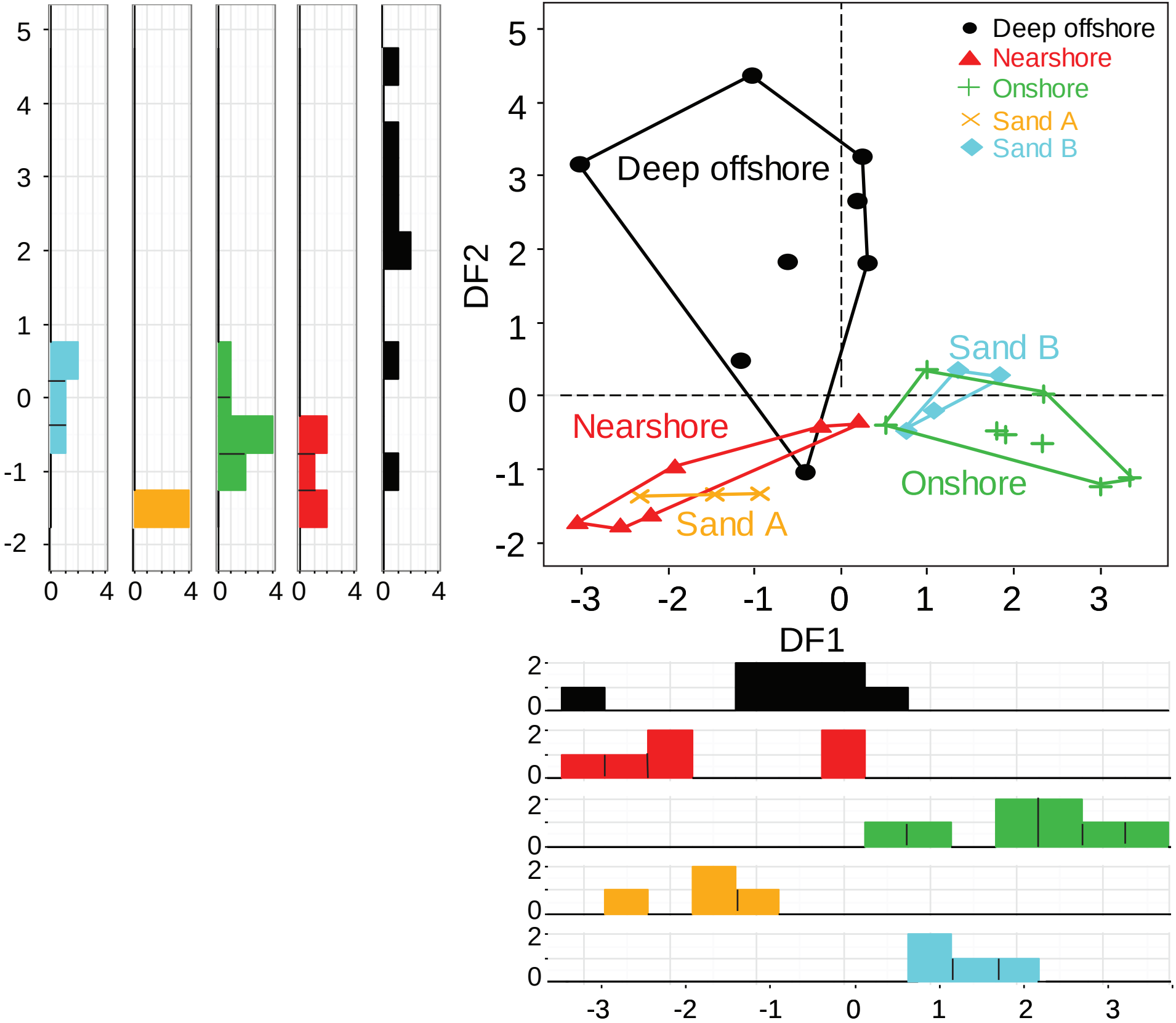
Deep offshore
Nearshore
Onshore
Sand A
Sand B
DF1
DF2

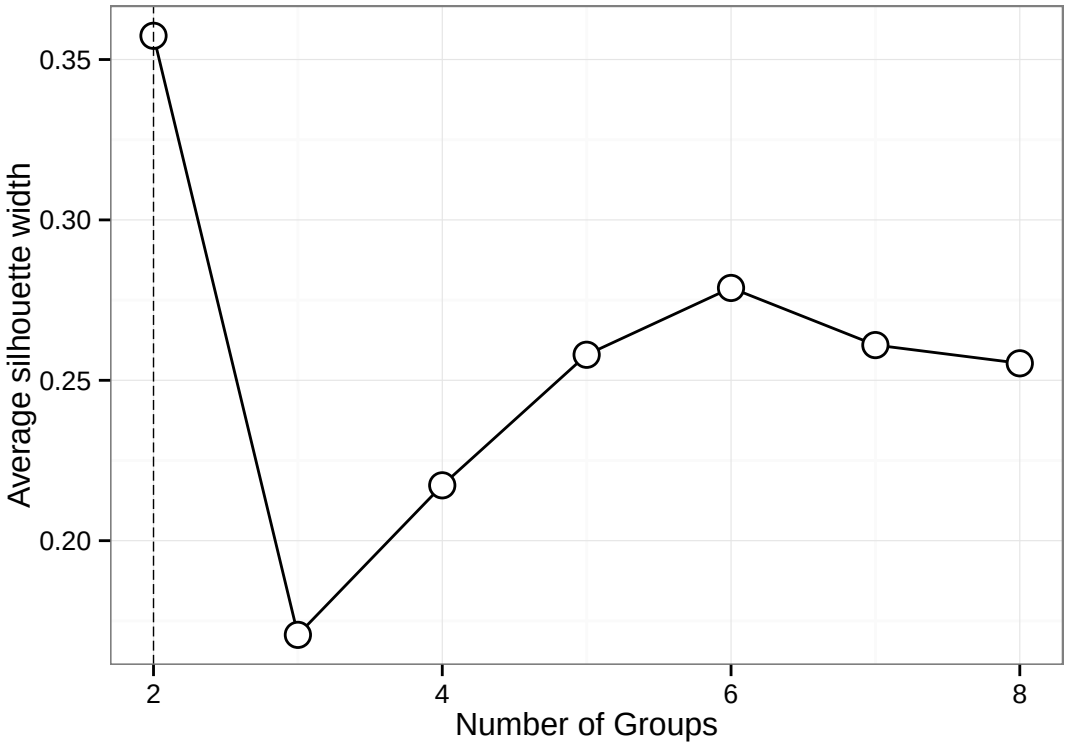
Average silhouette width
0.35
0.30
0.25
0.20
2
4
6
8
Number of Groups

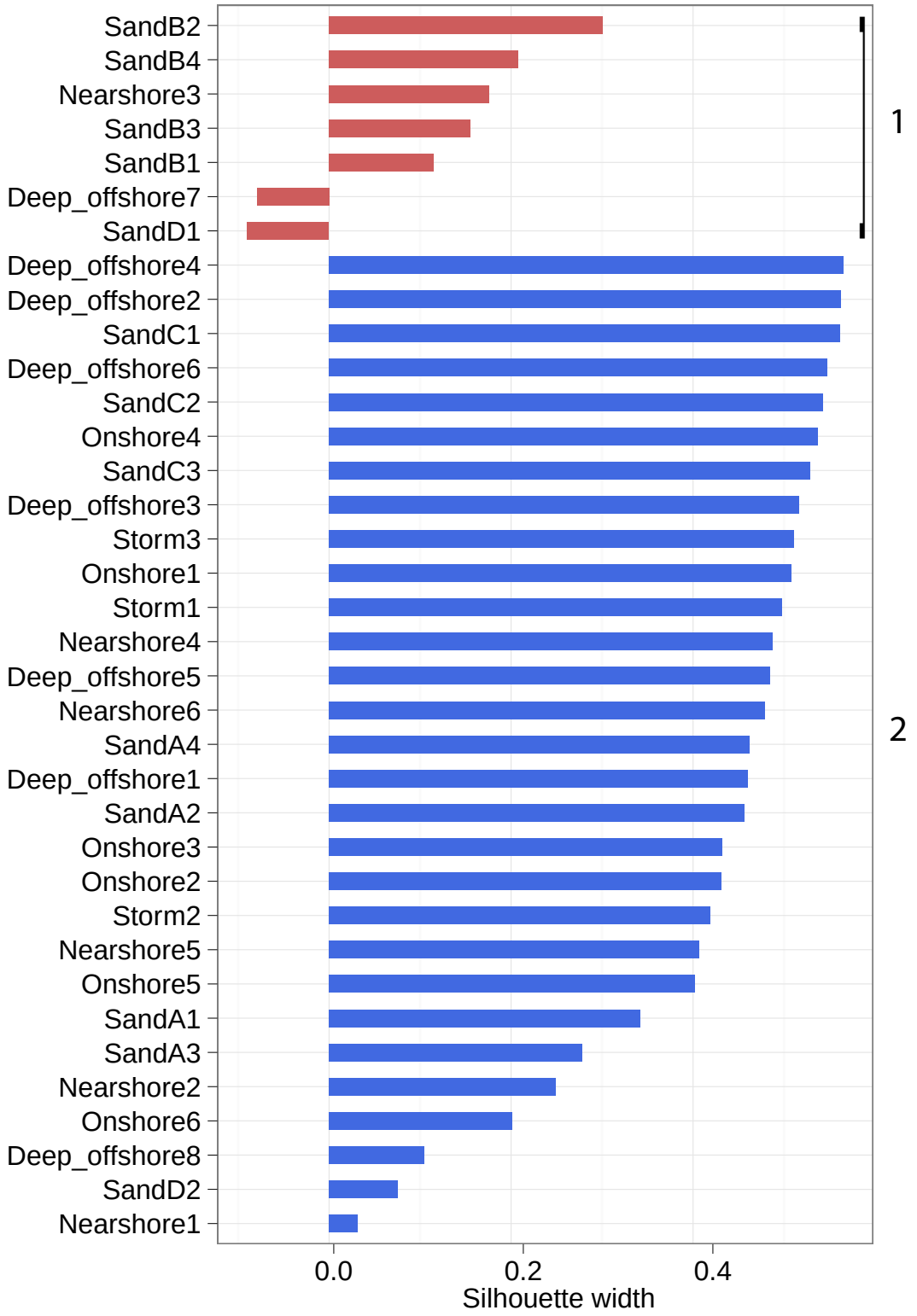
SandB2
SandB4
Nearshore3
SandB3
SandB1
Deep_offshore7
SandD1
Deep_offshore4
Deep_offshore2
SandC1
Deep_offshore6
SandC2
Onshore4
SandC3
Deep_offshore3
Storm3
Onshore1
Storm1
Nearshore4
Deep_offshore5
Nearshore6
SandA4
Deep_offshore1
SandA2
Onshore3
Onshore2
Storm2
Nearshore5
Onshore5
SandA1
SandA3
Nearshore2
Onshore6
Deep_offshore8
SandD2
Nearshore1
1
2
0.0
0.2
0.4
Silhouette width

Groups	Sample codes	Mean (phi)	Sorting	Skewness	Kurtosis	Description
Deep-Offshore	PT-OS 03	1.577	1.601	0.465	1.59	Medium sand, poorly sorted, very fine skewed, very leptokurtic
Deep-Offshore	PT-OS 05	1.218	0.782	0.105	0.962	Medium sand, moderately sorted, fine skewed, mesokurtic
Deep-Offshore	PT-OS 13	0.999	0.89	0.242	1.246	Coarse sand, moderately sorted, fine skewed, leptokurtic
Deep-Offshore	PT-OS 15	1.275	0.994	0.228	1.398	Medium sand, moderately sorted, fine skewed, leptokurtic
Deep-Offshore	PT-OS 17	0.842	0.951	0.318	1.293	Coarse sand, moderately sorted, very fine skewed, leptokurtic
Deep-Offshore	PT-OS 21	4.153	2.01	0.176	1.223	Very coarse silt, very poorly sorted, fine skewed,leptokurtic
Mean		1.67	1.2	0.25	1.28	
Nearshore	PT-OS 24	3.458	0.613	0.134	1.161	Very fine sand, moderately well sorted, fine skewed, leptokurtic
Nearshore	PT-OS 26	3.448	0.874	0.311	1.997	Very fine sand, moderately sorted, very fine skewed, very leptokurtic
Nearshore	PT-OS 28	3.021	0.527	0.014	0.935	Very fine sand, moderately well sorted, symmetrical, mesokurtic
Nearshore	PT-OS 32	2.798	0.527	0.002	0.935	Fine sand, moderately well sorted, symmetrical, mesokurtic
Nearshore	PT-OS 33	2.843	0.541	0.006	0.931	Fine sand, moderately well sorted, symmetrical, mesokurtic
Nearshore	PT-OS 34	2.202	1.164	0.044	0.784	Fine sand, poorly sorted, symmetrical, platykurtic
Mean		2.96	0.7	0.085	1.12	
Onshore	PT-02	1.971	0.557	0.01	0.938	Medium sand, moderately well sorted, symmetrical, mesokurtic
Onshore	PT-04	2.17	0.62	0.003	0.924	Fine sand, moderately well sorted, symmetrical, mesokurtic
Onshore	PT-05	1.856	0.57	0.004	0.937	Medium sand, moderately well sorted, symmetrical, mesokurtic
Onshore	PT-07	1.996	0.671	-0.012	0.94	Medium sand, moderately well sorted, symmetrical, mesokurtic
Onshore	PT-07(S)	1.24	0.639	0.027	0.921	Medium sand, moderately well sorted, symmetrical, mesokurtic
Onshore	PT-08	1.75	0.667	0.035	0.933	Medium sand, moderately well sorted, symmetrical, mesokurtic
Onshore	PT-09	1.692	0.62	0.021	0.932	Medium sand, moderately well sorted, symmetrical, mesokurtic
Onshore	PT-11	1.848	0.674	0.015	0.936	Medium sand, moderately well sorted, symmetrical, mesokurtic
Mean		1.81	0.63	0.01	0.93	
Sand A	PT-CT04 19	3.157	0.707	-0.068	1.061	Very fine sand, moderately sorted, symmetrical, mesokurtic
Sand A	PT-CT04 18	3.205	0.639	-0.064	0.989	Very fine sand, moderately well sorted, symmetrical, mesokurtic
Sand A	PT-CT04 11	3.052	0.812	-0.196	1.16	Very fine sand, moderately sorted, coarse skewed, leptokurtic
Sand A	PT-CT04 09	3.09	0.624	0.04	1.046	Very fine sand, moderately well sorted, symmetrical, mesokurtic
Mean		3.126	0.7	0.072	1.064	
SandB	PT-CTpaleo06	3.061	0.858	-0.239	1.247	Very fine sand, moderately sorted, coarse skewed, leptokurtic
SandB	PT-CTplaeo07	3.152	0.567	0.063	1.049	Very fine sand, moderately well sorted, symmetrical, mesokurtic
SandB	PT-CTpaleo11	3.165	0.585	-0.017	0.937	Very fine sand, moderately well sorted, symmetrical, mesokurtic
SandB	PT-CTpaleo10	3.028	0.657	-0.077	0.991	Very fine sand, moderately well sorted, symmetrical, mesokurtic
Mean		3.1	0.67	0.067	1.056	
SandC	SandC 1	2.696	1.188	0.008	1.63	Fine sand, poorly sorted, symmetrical, very leptokurtic
SandC	SandC 2	2.818	1.074	0.165	1.675	Fine sand, poorly sorted, fine skewed, very leptokurtic
SandC	SandC 3	2.839	1.039	0.18	1.706	Fine sand, poorly sorted, fine skewed, very leptokurtic
Mean		2.78	1.1	0.12	1.67	
SandD	SandD 1	1.315	0.961	0.24	1.092	Medium sand, moderately sorted, fine skewed, mesokurtic
SandD	SandD 2	1.557	1.164	0.287	1.115	Medium sand, poorly sorted, fine skewed, leptokurtic
Mean		1.44	1.06	0.26	1.1	
Storm	Storm 1	1.554	0.552	0.01	0.934	Medium sand, moderately well sorted, symmetrical, mesokurtic
Storm	Storm 2	1.588	0.605	0.016	0.926	Medium sand, moderately well sorted, symmetrical, mesokurtic
Storm	Storm 3	1.583	0.559	0.002	0.934	Medium sand, moderately well sorted, symmetrical, mesokurtic
Mean		1.57	0.57	0.01	0.93	

Groups	Sample codes	Quartz	Labradorite	Orthoclase	Microcline	Aragonite	Zircon	Cassiterite	Monazite	Kaolinite	Muscovite
Deep-Offshore	PT-OS 03	38.8	2.2	9.6	4.8	12.6	1.4	0.5	3.5	2.6	7.8
Deep-Offshore	PT-OS 05	44.0	2.0	16.1	10.1	13.7	5.3	0.7	3.0	0.9	3.8
Deep-Offshore	PT-OS 07	38.7	1.8	12.0	1.3	9.7	1.2	0.2	2.9	1.3	9.3
Deep-Offshore	PT-OS 13	59.9	0.5	10.5	5.7	6.4	3.1	0.7	2.2	1.7	6.2
Deep-Offshore	PT-OS 15	42.1	3.2	7.4	7.8	8.7	2.2	0.8	3.5	3.5	9.4
Deep-Offshore	PT-OS 17	40.1	2.9	10.5	10.5	10.1	4.5	1.7	4.2	1.8	6.7
Deep-Offshore	PT-OS 21	63.3	0.6	7.8	9.1	5.3	2.1	0.6	1.9	1.5	3.9
Deep-Offshore	PT-OS 22	64.7	1.6	9.1	8.2	5.3	2.4	0.6	1.5	1.9	2.0
Nearshore	PT-OS 24	65.5	0.8	9.3	6.7	9.2	3.4	1.1	1.4	0.8	1.6
Nearshore	PT-OS 26	56.3	0.5	12.5	8.4	11.4	4.2	1.1	2.3	0.6	2.7
Nearshore	PT-OS 28	46.5	1.1	14.5	9.5	11.1	6.6	0.9	2.6	1.7	4.8
Nearshore	PT-OS 32	61.1	0.7	12.4	7.6	7.4	4.1	1.0	1.9	1.1	2.8
Nearshore	PT-OS 33	78.4	0.3	7.5	5.2	3.3	2.4	0.4	1.5	0.6	3.1*
Nearshore	PT-OS 34	58.7	1.0	11.1	8.0	9.6	3.4	1.6	1.7	0.9	3.9
Onshore	PT-02	53.4	1.7	14.3	8.7	8.2	5.6	1.2	2.0	1.0	3.9
Onshore	PT-04	56.3	0.9	13.6	8.4	7.8	4.6	1.6	2.2	1.0	3.5
Onshore	PT-05	45.7	1.6	14.9	10.6	10.0	7.3	0.8	2.4	1.2	4.4
Onshore	PT-07	57.1	1.0	12.5	8.5	7.3	5.3	1.1	2.4	1.0	2.6
Onshore	PT-07 (s)	37.6	1.0	14.9	13.1	12.3	8.3	1.0	1.8	1.7	6.6
Onshore	PT-08	49.6	1.7	14.0	9.4	8.9	7.7	1.1	2.2	0.9	4.4
Onshore	PT-09	37.3	1.2*	12.7	9.4	9.2	13.5	3.8	1.3	2.6	6.6
Onshore	PT-11	47.8	0.5	10.7	8.2	6.7	12.3	3.1	1.4	1.4	5.7
SandA	PT CT 04 09	52.1	1.4	13.8	9.0	12.0	4.6	1.0	2.4	0.9	2.9
SandA	PT-CT 04 11	57.0	0.3	11.8	8.7	10.1	3.7	1.4	1.8	1.2	3.9
SandA	PT-CT 04 18	51.2	1.5	14.0	9.0	12.4	4.8	0.9	2.5	0.9	2.8
SandA	PT-CT 04 19	53.8	1.1	12.9	9.8	11.0	4.7	1.1	2.2	0.5	2.8
SandB	PT-CT 06 pal	44.6	2.6	13.6	10.8	11.0	6.3	0.6	2.9	1.3	4.9
SandB	PT-CT 07 pal	48.5	1.4	14.5	9.9	8.9	6.2	1.0	2.6	1.3	4.8
SandB	PT-CT 10 pal	53.2	1.4	13.3	8.5	9.2	6.7	1.0	2.4	1.2	3.1
SandB	PT-CT 11 pal	53.9	1.5	11.7	9.6	8.1	6.4	1.2	2.1	1.2	4.1

*: missing values, replaced by the mean of group

Groups	Sample codes	V	Cr	Ni	Cu	As	Se	Rb	Sr	Zr	Nb	Sn	Ba	La	Ce	Hf	Pb	Th	U	Y	Cs	Ga	Bi
Deep-Offshore	PT-OS 03	18.7	22.2	12.0	7.5	0.5	3.3	20.4	501.7	91.7	5.8	23.0	31.5	5.9	8.1	0.4	6.2	9.6	0.5	9.2	7.3	5.0	2.1
Deep-Offshore	PT-OS 05	7.0	13.2	5.5	5.8	0.5	2.9	19.8	356.2	50.1	3.0	7.2	24.8	6.7	0.7	0.5	3.3	5.4	0.5	5.6	2.0	2.4	2.1
Deep-Offshore	PT-OS 07	15.5	17.8	5.9	7.8	0.5	3.1	32.1	592.6	328.3	11.2	206.0	48.8	8.6	35.3	4.5	6.3	14.0	1.6	13.9	2.0	4.6	2.1
Deep-Offshore	PT-OS 13	9.7	8.4	5.6	6.1	3.2	3.4	10.3	184.8	119.5	8.4	35.6	22.3	7.1	10.9	3.6	3.4	9.2	0.5	8.6	2.0	3.0	2.2
Deep-Offshore	PT-OS 15	12.8	12.9	5.4	7.2	9.0	2.9	11.8	235.7	60.0	3.4	12.6	17.8	4.5	4.5	0.3	4.4	9.8	0.5	7.5	2.0	2.9	2.3
Deep-Offshore	PT-OS 17	10.3	12.3	7.0	6.8	3.0	3.9	11.1	204.2	57.4	4.5	35.2	1.5	10.8	13.1	1.7	3.0	7.7	0.5	6.8	2.0	3.0	2.9
Deep-Offshore	PT-OS 21	46.9	36.6	16.7	12.5	8.6	2.6	160.8	563.8	438.7	24.3	47.9	111.6	41.9	108.3	8.8	35.2	49.2	0.5	35.2	18.8	15.7	2.9
Deep-Offshore	PT-OS 22	44.0	39.8	12.5	10.1	17.2	1.4	100.7	729.6	306.6	17.5	45.9	84.9	12.5	66.3	7.6	28.8	33.6	4.8	27.2	2.0	10.3	1.9
Nearshore	PT-OS 24	5.0	15.1	9.9	8.5	1.0	3.1	117.8	601.8	1581.0	29.4	63.6	81.2	101.7	266.0	32.1	18.9	105.5	16.7	87.9	2.0	7.1	2.8
Nearshore	PT-OS 26	11.0	16.0	8.8	7.8	3.7	2.3	113.5	595.8	1144.0	24.4	52.6	75.6	82.5	183.0	24.4	21.1	80.4	10.4	69.8	2.0	7.2	2.6
Nearshore	PT-OS 28	5.4	16.9	11.8	8.6	0.5	3.5	63.7	345.9	2687.0	45.4	120.3	49.6	159.0	346.0	55.8	14.7	152.7	24.7	139.3	2.0	5.1	3.3
Nearshore	PT-OS 32	5.2	10.1	6.3	7.9	1.2	2.7	62.8	376.3	936.6	18.9	63.2	54.8	75.7	131.3	17.9	10.6	54.5	6.8	45.5	2.0	5.1	2.3
Nearshore	PT-OS 33	4.8	11.1	5.7	7.2	1.4	2.3	70.2	483.5	1269.0	21.6	91.3	58.8	67.3	181.4	23.7	12.1	81.3	9.9	61.6	2.0	4.5	2.0
Nearshore	PT-OS 34	6.7	12.4	5.3	7.2	2.0	2.1	64.6	406.6	1163.0	65.8	152.7	57.3	38.9	71.4	21.2	12.4	44.3	7.6	49.3	2.0	5.2	1.8
Onshore	PT-02	11.1	7.5	9.7	7.8	0.5	4.8	11.1	3.2	497.2	18.0	61.8	1.5	15.2	33.4	13.1	0.8	14.8	1.6	15.9	2.0	3.0	3.3
Onshore	PT-04	8.0	5.8	9.9	7.9	0.5	5.8	18.3	4.5	376.0	14.3	45.4	23.4	15.1	0.5	10.8	1.4	10.5	0.6	13.4	11.3	3.5	3.2
Onshore	PT-05	6.6	8.5	11.4	8.3	0.5	5.7	11.0	66.7	1062.0	48.2	100.2	1.5	33.5	63.6	22.7	2.6	26.5	5.9	35.0	2.0	5.0	3.5
Onshore	PT-07	5.4	7.8	6.3	10.3	0.5	4.4	20.9	108.9	703.5	34.4	64.6	26.8	17.5	0.5	14.0	3.9	12.8	3.9	19.3	2.0	4.1	2.6
Onshore	PT-07 (s)	0.5	13.0	6.8	12.3	0.5	4.4	10.0	127.8	1190.0	85.0	164.9	1.5	32.2	63.3	25.3	5.3	25.6	7.8	38.7	2.0	4.4	2.8
Onshore	PT-08	7.3	13.4	11.7	8.3	0.5	7.0	10.2	116.1	1536.0	116.6	273.3	21.6	38.5	95.6	35.2	5.6	34.1	9.5	55.0	2.0	6.7	4.2
Onshore	PT-09	0.5	25.6	9.7	7.2	0.5	1.9	8.6	92.6	4724.0	400.3	1276.0	15.4	105.6	253.0	94.2	22.7	97.1	31.7	170.4	2.0	5.1	0.5
Onshore	PT-11	0.5	23.1	11.1	7.5	0.5	3.5	11.7	127.3	5069.0	329.8	952.0	1.5	85.6	230.0	102.9	18.6	110.0	35.3	165.8	2.0	5.9	2.2
SandA	PT CT 04 09	16.0	16.0	11.0	9.0	0.5	6.6	81.0	488.0	831.0	22.0	64.0	63.0	48.0	104.0	20.0	1.0	46.1	9.2	41.0	3.5	8.0	0.5
SandA	PT-CT 04 11	13.5	12.7	6.0	8.6	1.8	1.2	81.2	495.6	906.7	23.8	78.8	64.0	50.0	108.6	20.3	13.5	47.9	10.9	44.7	2.0	2.9	0.5
SandA	PT-CT 04 18	13.9	14.0	5.9	14.4	0.5	2.3	83.2	468.4	937.3	24.0	79.6	62.4	46.1	103.9	17.9	13.6	51.8	11.8	46.3	11.8	6.0	2.2
SandA	PT-CT 04 19	11.7	16.1	5.7	8.8	0.5	1.4	82.0	535.8	820.2	21.8	65.5	60.1	48.3	101.3	17.8	13.8	44.9	9.9	42.1	2.0	3.3	0.5
SandB	PT-CT 06 pal	7.0	15.0	13.0	4.0	0.5	10.0	93.0	19.0	2134.0	35.0	144.0	70.0	162.0	379.0	53.0	1.0	159.7	20.2	117.0	3.5	8.0	0.5
SandB	PT-CT 07 pal	2.1	14.6	15.4	11.4	0.5	6.8	93.8	15.9	2192.0	35.6	152.8	76.1	174.6	362.0	49.1	15.8	165.8	21.7	118.4	10.3	7.8	4.9
SandB	PT-CT 10 pal	2.9	11.5	14.1	12.6	0.5	6.2	90.5	15.3	1818.0	35.1	137.2	66.2	122.1	278.0	41.0	14.1	129.6	17.5	96.6	2.0	8.2	4.3
SandB	PT-CT 11 pal	0.5	11.7	12.6	12.2	0.5	5.5	90.2	15.1	1895.0	35.3	150.3	64.7	141.9	281.7	41.2	14.5	135.4	19.1	100.7	8.7	7.0	3.8
SandC	SandC 1	3.0	9.0	6.0	6.0	0.3	3.0	37.0	7.0	196.0	7.0	28.0	52.0	15.0	35.0	4.0	5.0	8.4	1.1	10.0	3.5	4.0	2.0
SandC	SandC 2	1.0	6.0	5.0	5.0	0.3	3.0	29.0	5.0	121.0	4.0	9.0	42.0	1.0	15.0	3.0	4.0	6.3	1.0	7.0	3.5	3.0	2.0
SandC	SandC 3	4.0	10.0	6.0	6.0	0.3	3.0	70.0	20.0	609.0	13.0	39.0	67.0	39.0	72.0	13.0	12.0	31.1	4.1	30.0	3.5	5.0	2.0
SandD	SandD 1	0.5	17.0	7.0	5.0	0.3	3.0	10.0	30.0	2844.0	191.0	701.0	23.0	69.0	129.0	56.0	10.0	60.2	20.4	90.0	3.5	4.0	2.0
SandD	SandD 2	0.5	15.0	7.0	4.0	0.3	3.0	11.0	29.0	2679.0	155.0	443.0	23.0	71.0	121.0	53.0	9.0	49.4	16.5	86.0	3.5	3.0	0.5
Storm	Storm 1	0.5	10.1	7.2	5.7	0.3	3.1	62.8	15.0	779.5	16.0	52.0	66.5	62.9	83.8	15.9	10.9	40.6	6.6	34.4	3.5	4.8	2.0
Storm	Storm 2	0.5	14.5	5.6	7.2	0.3	3.0	11.5	26.9	1240.0	95.3	241.4	0.7	22.7	49.7	23.6	5.4	26.6	7.6	41.3	3.5	5.0	2.4
Storm	Storm 3	1.8	11.0	6.7	5.9	0.3	2.9	70.5	16.6	677.1	14.9	42.4	74.3	48.9	77.7	13.4	12.4	34.6	5.7	32.3	3.5	4.3	1.7